

LEAD(II) ADSORPTION ON THIOUREA TREATED GRAPHENE OXIDE IN
AQUEOUS SOLUTIONS

A THESIS SUBMITTED TO
THE GRADUATE SCHOOL OF NATURAL AND APPLIED SCIENCES
OF
MIDDLE EAST TECHNICAL UNIVERSITY

BY

GÜLİZ ERSOY ÖZMEN

IN PARTIAL FULFILLMENT OF THE REQUIREMENTS
FOR
THE DEGREE OF MASTER OF SCIENCE
IN
CHEMISTRY

JULY 2019

Approval of the thesis:

**LEAD(II) ADSORPTION ON THIOUREA TREATED GRAPHENE OXIDE
IN AQUEOUS SOLUTIONS**

submitted by **GÜLİZ ERSOY ÖZMEN** in partial fulfillment of the requirements for
the degree of **Master of Science in Chemistry Department, Middle East Technical
University** by,

Prof. Dr. Halil Kalıpçılar
Dean, Graduate School of **Natural and Applied Sciences**

Prof. Dr. Cihangir Tanyeli
Head of Department, **Chemistry**

Prof. Dr. Gülsün Gökağaç Arslan
Supervisor, **Chemistry, METU**

Assoc. Prof. Dr. Gülay Ertaş
Co-Supervisor, **Chemistry, METU**

Examining Committee Members:

Assoc. Prof. Dr. Emren Nalbant Esentürk
Chemistry, METU

Prof. Dr. Gülsün Gökağaç Arslan
Chemistry, METU

Assoc. Prof. Dr. Gülay Ertaş
Chemistry, METU

Prof. Dr. Metin Aydın
Chemistry, Ondokuz Mayıs University

Assoc. Prof. Dr. Ezel Boyacı
Chemistry, METU

Date: 30.07.2019

I hereby declare that all information in this document has been obtained and presented in accordance with academic rules and ethical conduct. I also declare that, as required by these rules and conduct, I have fully cited and referenced all material and results that are not original to this work.

Name, Surname: Gliz Ersoy zmen

Signature:

ABSTRACT

LEAD(II) ADSORPTION ON THIOUREA TREATED GRAPHENE OXIDE IN AQUEOUS SOLUTIONS

Ersoy Özmen, Güliz
Master of Science, Chemistry
Supervisor: Prof. Dr. Gülsün Gökağaç Arslan
Co-Supervisor: Assoc. Prof. Dr. Gülay Ertaş

July 2019, 78 pages

Lead poisoning has serious damages on the human health. The Pb^{+2} contamination in water affects the kidneys and nervous, cardiovascular, immune, reproductive and developmental systems resulting in Alzheimer's, Parkinson's and Schizophrenia diseases. One of the ways that human are exposed to lead is through water resources, therefore, removing lead from aqueous solutions is a significant issue in our everyday life. It is known that graphene oxide (GO) is a promising material to remove Pb^{+2} ions due to its high adsorption capacity. It is believed that treatment of GO by thiourea enhance the Pb^{+2} adsorption capacity due to raise in attachment points on the surface of the material. For this purpose, in this research GO and thiourea treated GO for 5 min (GO/TUT/5min), 40 min (GO/TUT/40min), 50 min (GO/TUT/50 min), 60 min (GO/TUT/60 min), 3 hours (GO/TUT/3 h), 24 hours at 70 °C (GO/TUT/24h) and 24 hours at 80 °C (r-GO) were prepared and characterized by FTIR, XRD and TGA. Their Pb^{+2} adsorption capacities were defined by ICP-MS. The adsorption capacities were found to be 1232 mg/g GO, 2042 mg/g GO/TUT/5min, 1891 mg/g GO/TUT/40min, 752 mg/g GO/TUT/50min, 1714 mg/g GO/TUT/60min, 1188 mg/g GO/TUT/3h, 1786 mg/g GO/TUT/24h and 763 mg/g r-GO. The observation of highest Pb^{+2} ion adsorption capacity for GO/TUT/5min might be due to existence of highest anchor

points on the surface of sample and alteration of stack structure into almost individual layer.

Keywords: Graphene, Graphene Oxide, Lead, Thiourea Functionalized Graphene Oxide, Lead in Aqueous Solutions

ÖZ

TİYOÜRE İLE MUAMELE EDİLMİŞ GRAFEN OKSİT ÜZERİNE SULU ÇÖZELTİLERDE KURŞUN (II) TUTTURULMASI

Ersoy Özmen, Güliz
Yüksek Lisans, Kimya
Tez Danışmanı: Prof. Dr. Gülsün Gökağaç Arslan
Ortak Tez Danışmanı: Doç. Dr. Gülay Ertaş

Temmuz 2019, 78 sayfa

Kurşun zehirlenmesinin insan sağlığı üzerine ciddi zararları vardır. Sudaki kurşun kirliliği insanlarda böbrekleri, sinir, kardiyovasküler, bağışıklık, üreme ve gelişme sistemlerini etkileyerek Alzheimer, Parkinson ve Şizofreni gibi hastalıklara yol açmaktadır. İnsanların kurşuna maruz kalma yollarından biri de su kaynaklarıdır ve bu nedenle kurşunun su kaynaklarından uzaklaştırılması oldukça önemli bir konudur. Grafen oksit (GO) yüksek kurşun adsorpsiyon kapasitesi nedeniyle kurşunu uzaklaştırmak için umut verici bir malzeme olduğu bilinmektedir. GO'nun tiyoüre ile muamele edilmesi sonucunda kurşunun tutunması için elverişli olan yüzeydeki tutunma noktalarını arttırdığı düşünülmektedir. Bu amaçla, bu araştırmada, GO ve 70°C'de tiyoüre ile 5 dakika (GO/TUT/5min), 40 dakika (GO/TUT/40 min), 50 dakika (GO/TUT/50 min), 60 dakika (GO/TUT/60 min), 3 saat (GO/TUT/3 h), 24 saat (GO/TUT/24h/70) ve 80°C'de 24 saat muamele edilmiş (r-GO) GO'ler hazırlanmış, FTIR, XRD ve TGA kullanarak karakterize edilmiştir. Hazırlanan bu maddelerin sulu çözeltilerde Pb⁺² iyonu tutma kapasiteleri ICP-MS kullanılarak tayin edilmiştir. Pb⁺² tutma kapasiteleri 1232 mg/g GO, 2042 mg/g GO/TUT/5min, 1891 mg/g GO/TUT/40min, 752 mg/g GO/TUT/50min, 1714 mg/g GO/TUT/60min, 1188 mg/g GO/TUT/3h, 1786 mg/g GO/TUT/24h ve 763 mg/g r-GO olarak bulunmuştur.

GO/TUT/5min'in en yüksek Pb^{+2} iyonu tutma kapasitesinin gözlenmesinin nedeni, maddenin yüzeyinde en yüksek tutunma noktalarının bulunmasından ve yığın yapının hemen hemen tek tek tabaka haline dönüşmesinden dolayı olabilir.

Anahtar Kelimeler: Grafen, Grafen Oksit, Kurşun, Tiyoüre ile Muamele Edilmiş Grafen Oksit, Sulu Çözeltilerde Kurşun

To my family and my lovely husband

ACKNOWLEDGEMENTS

I sincerely thank my supervisor Prof. Dr. Gülsün Gökağaç Arslan, for her guidance, support, help and encouragement during my thesis study. I appreciate her valuable thoughts both in classes and in life.

I sincerely thank my co-supervisor Assoc. Prof. Dr. Gülay Ertaş for her guidance, support and help during my thesis study.

I thank Canan Höçük and Sezin Atıcı for their helps with the ICP-MS measurements.

I thank Prof. Dr. Ayşen Yılmaz and her lab members especially Gencay Çelik for their help with the XRD measurements.

I thank Assist. Prof. Dr. Duygu Anaklı for her guidance through the synthesis procedures.

I thank Assoc. Prof. Dr. Salih Özçubukçu and his research group for being a lab next door and helping me whenever I needed.

I thank Dr. Aytül Saylam and Güzide Aykent for their guidance and helps during our coffee breaks.

I thank my friend Medine Soydan for her help and motivation since our senior year.

I thank Nanografi Nanotechnology Company in Teknokent ODTÜ where I worked as a R&D chemist, for their support in my thesis study especially I thank to Mehmet Başçı, Hüseyin Alagöz and Zafer Yiğit. I also thank them for giving me a chance to gain experience in the industry.

I thank Dr. Sara Samuie for her help and friendship in our lab.

I thank my family for always being there for me and giving me their endless support.

Lastly, I thank my lovely husband Göktuğ for his endless support, motivation and belief in me since we met.

TABLE OF CONTENTS

ABSTRACT	v
ÖZ	vii
ACKNOWLEDGEMENTS	x
TABLE OF CONTENTS	xi
LIST OF TABLES	xiv
LIST OF FIGURES	xv
CHAPTERS	
1. INTRODUCTION	1
1.1. Lead	1
1.1.1. Lead Poisoning and Its Effects on Human.....	1
1.1.1.1. Replacement of Pb^{+2} with Other Cations in the Human Body.....	2
1.1.1.2. Effect of Pb^{+2} on Heme Synthesis Pathway	3
1.1.1.3. Effect of Pb^{+2} on Embryo and Early Aged Children.....	3
1.1.2. Lead Contamination in Water	4
1.1.2.1. Adsorption of Pb^{+2} in Water via Nanomaterials.....	5
1.2. Graphene	7
1.2.1. Properties and Synthesis Methods of Graphene	8
1.3. Graphene Oxide.....	9
1.3.1. Chemically Functionalized Graphene Oxide.....	9
1.3.1.1. Graphene Oxide Functionalized with Nitrogen Containing Groups ..	10
1.3.1.2. Graphene Oxide Functionalized with Sulfur Containing Groups	10
1.4. Pb^{+2} Adsorption on GO Materials in the Literature	11

1.5. Aim of the Study	11
2. EXPERIMENTAL	13
2.1. Chemicals.....	13
2.2. Synthesis of Graphene Oxide.....	13
2.3. Synthesis of Thiourea Treated Graphene Oxide Materials	14
2.3.1. GO/TUT/5 min	15
2.3.2. GO/TUT/40min	15
2.3.3. GO/TUT/50min	15
2.3.4. GO/TUT/60min	15
2.3.5. GO/TUT/3h	15
2.3.6. GO/TUT/24h	16
2.3.7. r-GO.....	16
2.4. Characterization of Graphene Oxide.....	17
2.4.1. Fourier Transform Infrared (FTIR) Spectroscopy.....	17
2.4.2. X-ray Diffraction (XRD) Analysis.....	21
2.4.3. Ultraviolet Visible (UV-vis) Spectroscopy	24
2.4.4. Scanning Electron Microscopy (SEM).....	26
2.5. Thermogravimetric Analysis (TGA).....	29
2.6. Inductively Coupled Plasma Mass (ICP-MS) Spectroscopy	30
2.6.1. Preparation of Stock Pb ⁺² Solution	32
2.6.2. Preparation of Standard Samples	33
2.6.3. Sample Preparation for Pb ⁺² Adsorption on GO According to Time.....	33
2.6.4. Sample Preparation for Adsorption Capacity of GO with Different Concentrations of Pb ⁺² Solutions	33

2.6.5. Sample Preparation for Pb ⁺² Adsorption on GO/TUT Samples	34
3. RESULTS AND DISCUSSION	35
3.1. Characterization of Graphene Oxide	36
3.1.1. FTIR Spectrum of GO	37
3.1.2. UV-vis Spectrum of GO	38
3.1.3. XRD Spectrum of GO.....	39
3.1.4. SEM Images of GO.....	44
3.2. Characterization of Thiourea Treated GO Materials.....	45
3.2.1. FTIR Spectrum of GO/TUT Materials	45
3.2.2. XRD Spectrum of GO/TUT Materials.....	48
3.3. Thermal Gravimetric Analysis (TGA) Measurements	50
3.4. ICP-MS Measurements	54
3.4.1. Pb ⁺² Adsorption on GO Depending on Time.....	54
3.4.2. Pb ⁺² Adsorption Capacity of GO for Different Concentrations	57
4. CONCLUSION.....	65
5. FUTURE STUDIES	67
REFERENCES.....	69

LIST OF TABLES

TABLES

Table 2.1. Samples, exposure time with thiourea and temperature.	16
Table 3.1. Samples, treatment time with thiourea and temperature.	35
Table 3.2. Table showing mid- IR vibrations of functional groups.....	38
Table 3.3. Interlayer spacing, crystalline size and number of layers for GO	42
Table 3.4. XRD measurement results in the literature.....	43
Table 3.5. Interlayer distance, crystalline size and number of layers of GO samples	50
Table 3.6. Concentration of standard samples and their counts per second	55
Table 3.7. Adsorption of Pb ⁺² Samples on GO According to Time	56
Table 3.8. Weight of GO Samples.....	57
Table 3.9. Adsorption capacity of GO with different concentrations of Pb ⁺²	58
Table 3.10. Weight of GO/TUT samples.....	59
Table 3.11. Standard samples and their cps data	60
Table 3.12. Adsorption Capacities of GO/TUT samples.....	62
Table 3.13. Comparison of the results of this work with literature	63

LIST OF FIGURES

FIGURES

Figure 1.1. Zinc binding region of rat Amyloid- β precursor protein [5].	3
Figure 1.2. a) Zeolite structure showing cation exchange with Pb^{+2} ions [32]. b) MOF unit structure having metal ions as red, organic linkers as black and empty space is shown as yellow [33].	6
Figure 1.3. Figure showing structures of CNT, graphite and graphene from left to right.	6
Figure 1.4. a) Graphene (2D) forming b) fullerene (0D), c) carbon nanotubes (1D) and d) graphite (3D) [27].	7
Figure 2.1. Synthesis of graphene oxide.	14
Figure 2.2. Synthesis of thiourea treated graphene oxide materials.	16
Figure 2.3. Near, mid and far IR regions.	19
Figure 2.4. Optical diagram FTIR instrument [52].	20
Figure 2.5. X-ray diffraction from a sample [53].	22
Figure 2.6. Schematic diagram of XRD instrument [54].	22
Figure 2.7. Block diagram of UV-vis spectrometer.	24
Figure 2.8. Figure showing the reflection and scattering of light in a sample in a transparent cell [53].	25
Figure 2.9. Regions showing the electron-sample interaction [53]	28
Figure 2.10. Schematic diagram of SEM instrument [57]	29
Figure 2.11. Schematic diagram of ICP-MS instrument [70].	32
Figure 3.1. Representative structure of GO [38,87].	36
Figure 3.2. FTIR spectrum of GO.	37
Figure 3.3. UV-vis spectrum of GO	39
Figure 3.4. XRD spectrum of GO.	40
Figure 3.5. SEM images of GO.	44

Figure 3.6. FTIR spectrum of GO/TUT materials with respect to treatment time with thiourea	46
Figure 3.7. <i>FTIR spectrum of selected GO/TUT samples with thiourea</i>	47
Figure 3.8. Thiourea functionalized GO structure [87]	47
Figure 3.9. Mechanism of thiourea attachment on GO [43].....	48
Figure 3.10. TGA plot of GO samples, thiourea and graphite.	51
Figure 3.11. a) TGA plot of graphite, r-GO, GO/TUT/24h, GO and thiourea, b) Differential thermal analysis plot of GO.	52
Figure 3.12. TGA plot of GO/TUT samples, GO.....	53
Figure 3.13. TGA plot of GO/TUT samples treated at 70°C.	53
Figure 3.14. Graph of standard solutions cps vs concentration.....	55
Figure 3.15. Graph showing adsorption of Pb ⁺² on GO depending on time	57
Figure 3.16. Adsorbed mg Pb ⁺² / g GO vs concentration graph.....	59
Figure 3.17. Standard samples cps vs concentration graph	61

CHAPTER 1

INTRODUCTION

1.1. Lead

Lead is a heavy metal with blue-gray color which can be found naturally in Earth's crust by combination with other elements [1]. Lead is found in ores in the form of galena (PbS), anglesite (PbSO₄), cerussite (PbCO₃) and minim (Pb₃O₄) [1]. Density of lead is 11.34 g/cm³ [2]. It has a melting point of 327.43°C and boiling point of 1751°C [2]. It was first used in pottery as glaze and in medicine in ancient Egypt and China, followed by its usage in pipes, coins, jewelry, wine sweetener and writing equipment in times of Roman Empire [1]. Its usage became significantly popular after industrial revolution [3]. Lead is used as an additive in electrical and telephone cable covering to resist corrosion [1-3]. It is also used in printing, painting and ceramics for coloring, glazing and faster drying [1,3]. It is used in lead acid storage batteries, glass manufacturing to make crystal and leaded glass and it was used as an anti-knocking agent in gasoline in the past [1,3]. It is also used for protection from nuclear radiation due to its high density and its used in weaponry due to its malleability and softness [1,3]. However, besides these properties, lead is a toxic metal for the environment and human health.

1.1.1. Lead Poisoning and Its Effects on Human

Lead is known to be toxic to the human health and the environment for a very long time [4]. There are several studies that investigate the molecular mechanism of lead in the human body which concludes that lead poisoning has serious damages on the kidneys, nervous, immune, reproductive, developmental and cardiovascular systems [4,5].

1.1.1.1. Replacement of Pb^{+2} with Other Cations in the Human Body

In 1998, B. Fowler stated that after lead inhibition of rats, the lead goes through blood and accumulates in the brain and kidney [4]. This occurs by the replacement of zinc cations bound to the specific proteins that are rich in aspartic and glutamic dicarboxylic amino acids [4]. The structure of zinc binding region of rat Amyloid- β which was determined by NMR study as shown in Figure 1.1 [5]. In the figure, the round shape represents zinc divalent cation and it is surrounded by the Amyloid- β protein [5]. In addition to rat, monkey and catfish liver were also examined and both showed the same effects [6]. B. Fowler and his group also studied the lead-binding proteins in the cytosol in the human brain tissue to examine the binding of lead to low molecular weight proteins instead of the significant ones in the human body [6]. It is discovered that lead poisoning occurs via substitution of lead divalent ion as a result of competition with other divalent ions in the human body especially Ca^{+2} , Zn^{+2} , and Fe^{+2} [5]. In 1986, E. Habermann and his group proved that Pb^{+2} has a higher affinity for Calmodulin [7]. Calmodulin is an acidic calcium binding protein with low molecular weight [7]. Ca^{+2} binds to calmodulin in the cell cytoplasm [7]. Ca^{+2} plays an important role in releasing neurotransmitters from presynaptic nerve endings [8]. It is a significant process that Pb^{+2} mimics the action of Ca^{+2} and prevents releasing neurotransmitters [8]. Several studies showed that lead also competes for the zinc-binding sites in the zinc-finger proteins which are important for DNA replication, transcription and translation [4,9]. Pb^{+2} competes with Zn^{+2} to bind to the protein resulting in an alteration in protein structure [9]. Ordemann et al. and Richardt et al. reported that Pb^{+2} has a higher affinity than Zn^{+2} and Ca^{+2} in binding proteins [5,7]. In 2005, H. A. Godwin et. al. reported that lead bind to the proteins in a trigonal pyramidal geometry while zinc binds in a tetrahedral geometry. This alternation of geometry changes the folding type of protein which will reduce the probability of binding protein to DNA structure [10].

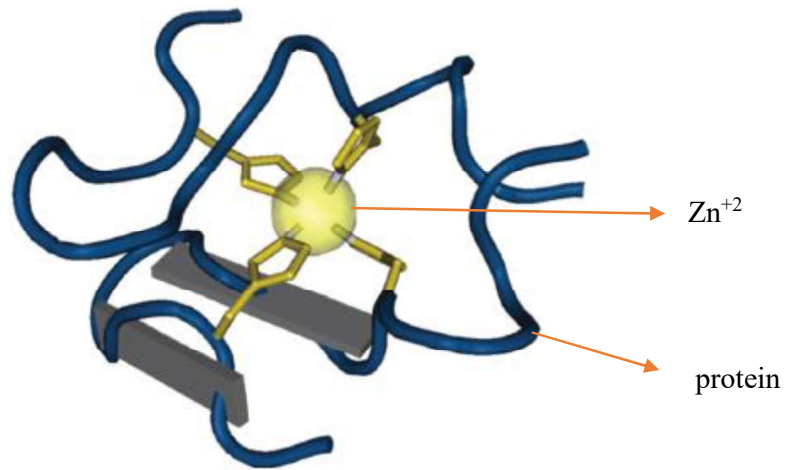


Figure 1.1. Zinc binding region of rat Amyloid- β precursor protein [5].

1.1.1.2. Effect of Pb^{+2} on Heme Synthesis Pathway

Lead has a significant effect on the heme synthesis pathway by binding to the enzyme δ -aminolevulinic acid dehydratase (ALAD) [6]. ALAD enzyme is very important in the human body, since it is involved in the heme production mechanism [6]. Heme is an important component of hemoglobin which is a member of hemoproteins [11]. Hemoglobin has a major role in the human body because it carries oxygen in the blood. Heme production is a multi-step process that requires eight different enzymes. ALAD enzyme is responsible for the second step of heme production process [11,12]. It catalyzes the asymmetric condensation of two δ -aminolevulinic acids (ALA) molecules to form one of porphobilinogen molecules which is a rate determining step in heme synthesis [11].

1.1.1.3. Effect of Pb^{+2} on Embryo and Early Aged Children

Gillis et al. reported that after lead (II) enters through respiratory and gastrointestinal systems, it stays in the blood for 30-35 days and then accumulates in brain, lungs, liver, teeth, and bones for 20-30 years [12,13]. The U.S. Centre for Disease Control established the concern limit for blood lead concentration level as $10\mu\text{g}/\text{dl}$ for children [12]. According to R. Goyer, another significant damage of lead

is to the embryo through the trans placental transport from mother to fetus [14]. Lead passes through the placenta and contaminates breast milk. Elevated blood lead levels of a mother can cause miscarriage, prematurity, low birth weight and retardation of the embryo [14,15]. In 2010, Vigehe et al. found out that higher blood lead concentrations such as $4.52 \pm 1.53 \mu\text{g/dl}$ were seen in preterm mothers rather than full-term mothers [16]. Early ages of exposure to lead are also, critical. Since the nervous system is developing at early ages, according to researchers, children with high exposure to lead may have lower IQ levels [12,14].

1.1.2. Lead Contamination in Water

Lead can be found in both natural groundwater and surface water. Source of its appearance may result from both natural processes like soil erosion or human activities like mining [17]. According to the researches, Turkey is one of the countries in which there is lead contamination in water [18]. There are several reasons for this contamination. First, there are still lead pipes used in old houses in Turkey. In 2005, Tuzen et al. investigated several tap water samples from Tokat in Turkey and found out that the lead concentration range was $3.1-7.7 \mu\text{g/l}$ which is critical since the World Health Organization (WHO) set the allowable lead concentration as $10 \mu\text{g/l}$ in tap water [18]. The highest level of lead was found in the industrial area of Tokat and it is concluded that lead contamination in water is related with the industrial activities in this area and other high lead contamination values are explained by the usage of lead pipes in houses [18]. In 2002, Soylak et al. studied the lead contamination levels in several areas near Yozgat in Turkey and found that the lead concentration level as $0.18-0.99 \mu\text{g/l}$ which is in the acceptable range [19]. They found that the highest value is in the urban areas resulting from the combustion of leaded petrol [19]. The lead contamination in water also affects the lead concentration in sea animals. In 2005, Celik and Oehlenschlaeger investigated several fishy product brands for heavy metal contamination and reported that frozen anchovy and canned tuna fish had the highest lead contamination values [20]. Keskin et al., 2007, examined a hundred seafood species in the Marmara Sea in Turkey and reported that all of these species have

acceptable lead contamination values. [21] According to this research, the most lead contaminated species are mussel, witting, striped bream, Atlantic bonito and blue fish with lead contamination values respectively; 0.822 ± 0.10 , 0.207 ± 0.03 , 0.269 ± 0.06 , 0.228 ± 0.02 , 0.270 ± 0.04 mg/kg [21]. According to the Turkish Food Codex Regulation, acceptable lead concentration in seafood is 1.0 mg/kg [21]. The high concentration levels of lead in water and seafood effects directly effects the lead concentration in the human body. Therefore, the lead contamination in water must be at an acceptable level.

Lead contamination in water is also a major problem around the world. In 2014, Flint, Michigan in USA people experienced a contamination in water [22]. The water source was changed from the Detroit Water to Flint River, however, according to the researchers, when the switch was made, chemicals added to water which were used for preventing corrosion were not added to the water [22]. This gave a result with lead contamination from the old pipes in houses [22]. Ziets et al., 2001, analyzed several water supplies from houses in Germany and stated that the concentration of lead is about 3.1 % of the water supplies was higher than 0.01 mg/l which is the maximum allowed value of lead in tap water by WHO [23].

1.1.2.1. Adsorption of Pb^{+2} in Water via Nanomaterials

Since lead is toxic and not biodegradable, it should be removed from water resources due to the toxic effect of lead to human health. There are several methods for removing lead in aqueous solutions such as adsorption [24], precipitation [24], ion exchange [24], filtration [24], oxidation [25], coagulation and flocculation processes [25]. Adsorption is one of the most attractive methods among them due to the flexibility of the process, availability of various materials to be used for adsorption and ease of desorption if necessary [25]. There are several materials used for the adsorption of Pb^{+2} from the sample. The most used ones are zeolites, metal organic frameworks (MOF), activated carbon, carbon nanotubes, graphene and graphene oxide [25, 26]. Zeolites have sodium, potassium and calcium ions in their structure

which are exchangeable with the lead ions in aqueous solutions via cation exchange mechanisms as shown in Figure 1.2a. [27]. MOFs form network structure by connecting metals on the centers with organic linkers and exchange with lead ions in aqueous solutions by cation exchange process as shown in Figure 1.2b. [28, 29]. Additionally, activated carbon can be used for removing lead ions in aqueous solutions. Activated carbon is derived from charcoal by pyrolysis and it removes metal ions by precipitation. Metal ions are adsorbed on activated carbon surface and precipitate as metal hydroxides to remove from the surface of the sample [30]. Carbon nanotubes (CNTs) and graphene are the other materials used for removing lead in aqueous solutions by adsorption. CNTs are the rolled form of a graphene sheet and when they are functionalized with oxygen groups, and as a result their lead adsorption capacity increases [31].

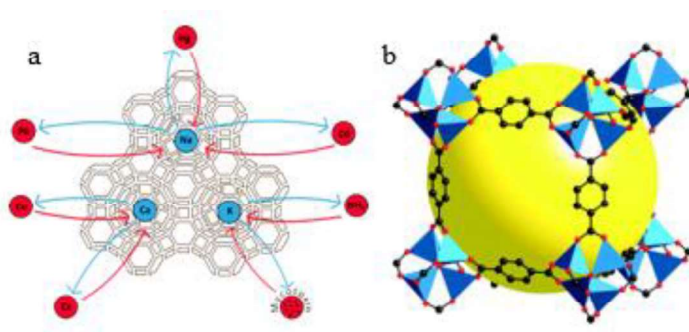


Figure 1.2. a) Zeolite structure showing cation exchange with Pb^{+2} ions [32]. b) MOF unit structure having metal ions as red, organic linkers as black and empty space is shown as yellow [33].

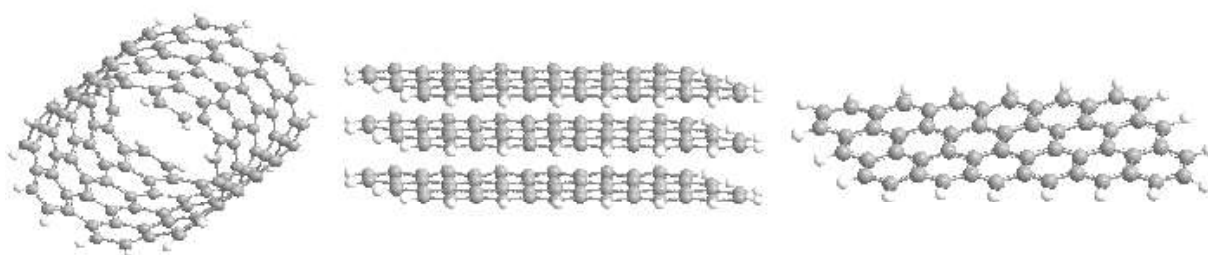


Figure 1.3. Figure showing structures of CNT, graphite and graphene from left to right.

1.2. Graphene

Graphene is a single layer of graphite and it was first experimentally obtained in 2004 by A. Geim and K. Novoselov by ‘Scotch Tape Method’ [34]. In this method simply graphene layers were separated from bulk graphite by the help of scotch tape [34]. Graphene has a honeycomb structure and all carbon atoms are in sp^2 hybridization [34]. When graphene is rolled up it forms zero dimensional fullerene and one dimensional carbon nanotubes [34]. Structure of graphene, graphite and the compounds that can be formed using graphene seen in Figure 1.4.

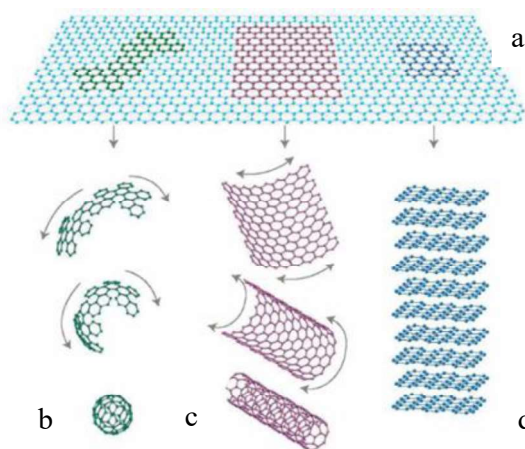


Figure 1.4. a) Graphene (2D) forming b) fullerene (0D), c) carbon nanotubes (1D) and d) graphite (3D) [27].

The studies on graphene began in 1859 with Benjamin Collins Brodie [35]. He studied the difference between amorphous and lamellar graphite and they showed different solubilities in strong acids [36]. He also reported the atomic weight of graphite as 33g/mol [36]. In 1918 using powder diffraction Kohlschütter and Haenni described the structure of graphite [35]. In 1947 Peter Wallace studied the band theory of graphite and he suggested that graphite may consist of single layers [35]. In 1987, Mouras et al. first reported the term ‘graphene’ meaning that graphite was made of several layers [37].

1.2.1. Properties and Synthesis Methods of Graphene

Graphene is a popular material due to its unique characteristic properties. Graphene has high electrical conductivity with high charge carrier mobility of $200\,000\text{ cm}^2\text{ V}^{-1}\text{ s}^{-1}$ and it is described as a zero bandgap semiconductor as the conductance and valance bands touch at a point in Brillouin zone [38]. It is found experimentally that graphene is stronger than steel with a Young Modulus of 1 TPa for monolayer graphene with 0.335 nm thickness [39]. Graphene has a high thermal conductivity at room temperature as $5000\text{ W m}^{-1}\text{ K}^{-1}$ [38]. The sigma bonds between carbon atoms in graphene are one of the strongest bonds and the pi bonds that are out of the plane in the graphene structure contribute to the delocalization of pi electrons [38]. Delocalization of pi electrons is important for the electrical conductivity of graphene [40]. There are also weak van der Waals interactions between the layers of graphene [40]. According to the researchers, monolayer graphene is transparent and its absorption is approximately 2.3% in visible range of EMR [40].

Graphene can be synthesized by two approaches as a) top-down and b) bottom-up [38]. According to the top-down approach, graphene was synthesized by breaking apart graphite layers by overcoming the interlayer van der Waals forces [38]. In this process, during the exfoliation of layers, the damage and agglomeration of layers are not wanted [38]. To separate the layers from each other micromechanical cleavage known as ‘scotch tape’ method, electrochemical exfoliation, exfoliation of graphite intercalation compounds, solvent based exfoliation, exfoliation of graphite oxide, arc discharge and unzipping carbon nanotubes [38]. The second approach, electrochemical exfoliation, is the bottom-up approach [38]. According to this approach, graphene is synthesized from different sources including carbon in their matrix [38]. The most used methods for this approach are epitaxial growth on silicon carbide and chemical vapor deposition (CVD) [38].

Graphene is hydrophobic and it has a structure consisting of only carbon and hydrogen bonds. Since heavy metal ions cannot adsorb to carbon and hydrogen

moiety, it is hard to use graphene for metal adsorption in water. Therefore, modifying it by several methods can provide many useful materials such as graphene oxide, graphite oxide, and reduced graphene oxide which contain oxygen groups that attracts the metal ions by their negative surface charges [40].

1.3. Graphene Oxide

Graphene can be oxidized with strong acids and oxidizing agents to form graphene oxide. Although it is challenging to determine the exact structure of graphene oxide, it is known that there are several oxygen containing groups on graphene oxide such as alcohols, epoxide, ketone and carboxyl groups which disrupt the aromaticity of graphene. Graphene oxide synthesis began in 1859 by Brodie et al. by using potassium chlorate (KClO_3) and then in 1898 Staumandier et al. used both concentrated sulfuric acid (H_2SO_4) and fuming nitric acid (HNO_3) with chlorate to perform one pot synthesis [41]. In 1958, Hummers and Offeman synthesized graphitic oxide by mixing graphite with sodium nitrate in sulfuric acid continued with the addition of potassium permanganate, distilled water, and hydrogen peroxide. They also reported that the color of the suspension at the end is a distinguisher for the degree of the oxidation. The color of suspension is light yellow, which shows the high degree of oxidation [42]. In 2010, Tour et al. synthesized graphene oxide by using an improved Hummers method which is known as Tour method [41]. In this method, graphene oxide was synthesized by mixing graphite flakes with 9:1 ratio of mixture of concentrated sulfuric acid and phosphoric acid continuing with slow addition of potassium permanganate followed by pouring this solution onto the ice and adding hydrogen peroxide [41]. This method increases the degree of oxidation of graphene compared to that of Hummers method [41].

1.3.1. Chemically Functionalized Graphene Oxide

There are several studies on chemically modified graphene oxide samples to increase their chemical, electrical and physical properties [41,42,43]. Chemical functionalization is defined as covalently bonding new functional groups to graphene

oxide structure, for instance sulfur, nitrogen, phosphorous and boron are mostly preferred atoms for chemical functionalization of graphene oxide due to their availability of lone pairs when attached to graphene oxide [43].

1.3.1.1. Graphene Oxide Functionalized with Nitrogen Containing Groups

In order to add nitrogen atom to the structure of graphene oxide, the surface is functionalized with groups such as $-NH_2$, $-NH$, $-C-N$, $-C=N$ using ammonia or amines as cystamine [44]. In these type of reactions adding nitrogen containing groups is followed by reduction of graphene oxide due to the release of oxygen groups [44]. Adding nitrogen containing compounds changes the surface of graphene oxide, the hybridization type and porosity of the sample [44]. It was reported that, functionalizing graphene oxide with nitrogen enhances heavy metal adsorption from the water [44,45].

1.3.1.2. Graphene Oxide Functionalized with Sulfur Containing Groups

According to the literature, functionalizing graphene oxide with sulfur containing groups such as; $-S-H$, $-S=O$, $-C-S$, $-C=S$ and $-C-SH$ increases the heavy metal adsorption capacity [46]. Several compounds can be used as sulfur sources such as sulfur nanoparticles, H_2S , Na_2S , K_2S , dimethyl sulfide, thiourea, sulfur containing polymers, proteins, and acids [43,44,46]. According to the literature, sulfur containing groups increase surface polarity by enhancing negative charge on graphene oxide, therefore, this compound attracts positively charged metal cations much stronger. According to the Pearson's Hard and Soft Acid Base Theory, the sulfur atom is a soft base and Pb^{+2} cation is a border line acid so sulfur atom will attract lead ions much strongly [46]. Therefore, research on graphene oxide functionalized with sulfur containing atoms attracted attention in the last years.

1.4. Pb⁺² Adsorption on GO Materials in the Literature

In the literature, there are a lot of studies on the adsorption capacities of Pb⁺² on different samples. Some of them are given here, for instance, Olanipekun et al. investigated the adsorption of lead on graphene oxide which was synthesized by the Hummers method and the maximum adsorption was found to be 30.13 mg Pb⁺²/ g GO [47]. Raghubanshi et al. worked on the same subject but in this case, GO was synthesized by the variations of Hummers method and Tour method and the best adsorption capacity was observed for GO synthesized by the Tour method as 120 mg Pb⁺²/ g GO [48]. In addition to these, Peng et al. examined Pb⁺² adsorption on GO synthesized by different type of graphite samples such as; flaky (GO-FG), lump (GO-LG) and amorphous (GO-AG) and the maximum adsorption capacity was found to be 789.9 mg Pb⁺²/ g GO-AG [49]. Sitko et al. researched on GO synthesized by potassium dichromate (K₂Cr₂O₇) and 1119 mg Pb⁺²/ g GO adsorption capacity were reported [50]. Zhao et al. also studied on a few layered GO which was synthesized by Hummers method and the result was 842 mg Pb⁺²/ g GO [51].

1.5. Aim of the Study

As stressed at the beginning of the chapter, Pb⁺² is a toxic and non-biodegradable ion [4]. It disrupts the release of neurotransmitters and makes an alteration in the zinc binding sides of proteins [4,9] which causes Alzheimer, Parkinson, Schizophrenia and anemia [4, 11]. Therefore, removing Pb⁺² ion from water is very important for creatures. For this purpose, in this study graphene oxide (GO), GO/TUT/5min, GO/TUT/40min, GO/TUT/50min, GO/TUT/60min, GO/TUT/3h, GO/TUT/24h and r-GO were synthesized, characterized and their Pb⁺² adsorption capacities were defined.

CHAPTER 2

EXPERIMENTAL

2.1. Chemicals

Graphite (5-10 μm , 99.9%) (Nanografi Nanotechnology Company Ankara, Turkey), $\text{Pb}(\text{NO}_3)_2$ (99.5%, Riedel de Haen Ag Seelze Hannover), H_2SO_4 (95-97%, Merck), H_3PO_4 (85%, Merck), KMnO_4 (high purity crystal, Merck), H_2O_2 (30%, Merck), Thiourea (99%, Sigma Aldrich), HBr (47%, Merck), HCl (37%, Merck), Ethanol (96%, Merck) were used without any purification. 18.0 M Ω deionized water was used in the preparation of all the samples using Millipore Pure Lab Option Q.

2.2. Synthesis of Graphene Oxide

Graphene oxide was synthesized by Improved Hummers Method which is also known as Tour Method [41]. In the first step, 0.75g of graphite was mixed with 90 ml of concentrated H_2SO_4 (95-97%) and 10 ml of concentrated H_3PO_4 (85%) in a 250 ml beaker in an ice bath and stirred for 30 min on a magnetic stirrer at 0°C. 4.5 gram of solid KMnO_4 was slowly added to the beaker while it is still in an ice bath and a green color was observed due to the Mn^{+2} ions in the solution [41]. In the second step, the solution was stirred on a magnetic stirrer at 50°C for 15 hours and the color of the solution was changed from black to light brown and it became slurry. In the third step, 100 ml of ice which was measured before freezing was put in a 600 ml beaker and the brown and slurry solution poured on to ice slowly. Then, it was stirred on a magnetic stirrer at room temperature until the bubbling stops and dark pink color occurs. In the fourth step, 10 ml 30% H_2O_2 solution was added slowly and the solution turns from dark pink to yellow which shows graphene oxide formation. The solution was stayed overnight, and in the last step, the solution was decanted and washed with a) 50 ml 30% HCl solution, b) 500 ml DI water, and c) 100 ml ethanol using centrifuge. Finally,

the prepared GO was dried in an oven at 70°C for 24 hours. The schematic representation of the synthesis procedure can be seen in Figure 2.1.

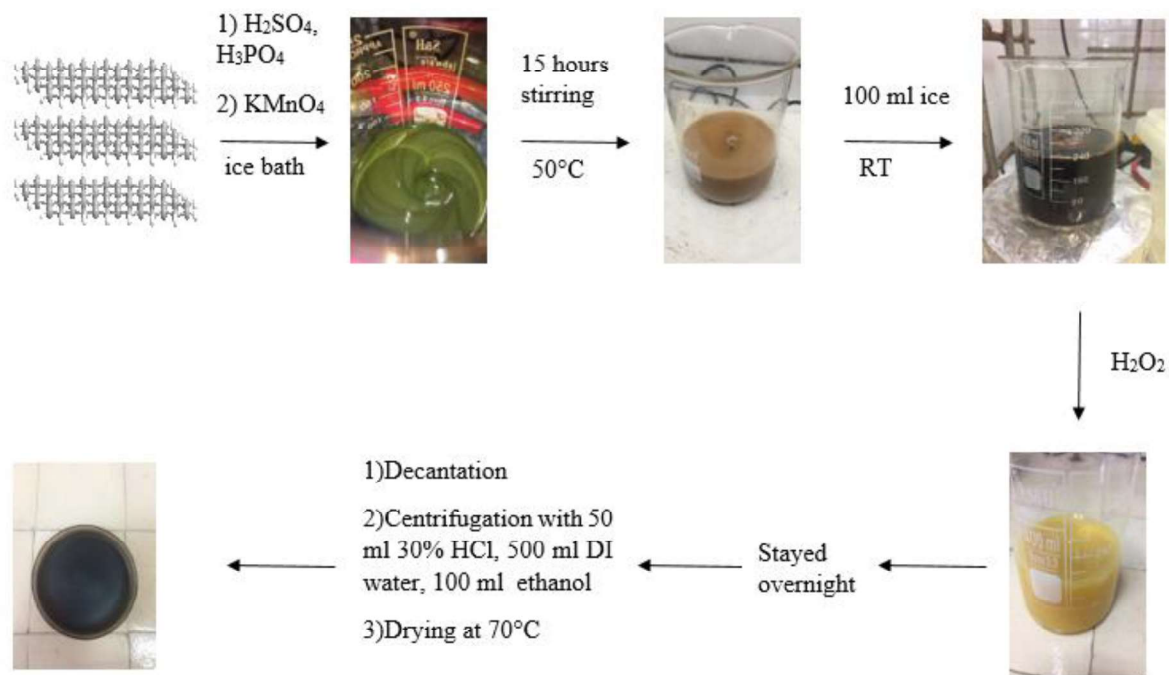


Figure 2.1. Synthesis of graphene oxide.

2.3. Synthesis of Thiourea Treated Graphene Oxide Materials

Thiourea treated GO (GO/TUT) samples were synthesized according to a procedure in the literature with several modifications such as different temperature and addition of NaOH [43]. Chua et al. synthesized r-GO by treating GO with thiourea for 24 hours at 80°C and then adding NaOH [40]. However, in this study after treating GO with thiourea, NaOH was not added to obtain thiourea functionalized GO which we called thiourea treated GO. Also, Chua et al. done the experiment at 80°C but in this work the temperature lowered to 70°C to slow down the reaction. For the first time, different thiourea treatment time is studied in this work, for instance 5 min, 40 min, 50 min, 60 min, 3 hours and 24 hours and they were called as GO/TUT/5min,

GO/TUT/40min, GO/TUT/50min, GO/TUT/60 min, GO/TUT/3h and GO/TUT/24h. In addition to these, reduced GO (r-GO) was also prepared for comparison. The treatment time with thiourea and temperature parameters are shown in Table 2.1.

2.3.1. GO/TUT/5 min

0.1 gram of GO was dispersed in 100 ml DI water in ultrasonic bath (Bandelin Sonorex RK 100) for 1 hour and heated to 30°C in a round bottomed flask. A 6.7 ml of concentrated HBr (47%) was added to this solution and stirred for 2 hours at this temperature. Then, the temperature was slowly increased to 70°C and 0.67 g of thiourea was directly added to the solution and stirred for 5 min. The sample solution was filtered and washed with 500 ml DI water by vacuum filtration through a 0.45 µm nitrocellulose filter paper. Finally, the filtrated solid was dried in oven at 70°C for 24 hours to obtain 5 min thiourea treated GO shown in Figure 2.2, which represented as GO/TUT/5min in Table 2.1.

2.3.2. GO/TUT/40min

40 minutes thiourea treated GO, GO/TUT/40min, was prepared by the same procedure as for GO/TUT/5 min, but in this case, the stirring time at 70°C is 40 min after addition of 0.67g of thiourea.

2.3.3. GO/TUT/50min

50 minutes thiourea treated GO, GO/TUT/50min, was prepared by the same procedure as for GO/TUT/5 min, but in this case, the stirring time at 70°C is 50 min after addition of 0.67g of thiourea.

2.3.4. GO/TUT/60min

60 minutes thiourea treated GO, GO/TUT/60min, was prepared by the same procedure as for GO/TUT/5 min, but in this case, the stirring time at 70°C is 60 min after addition of 0.67g of thiourea

2.3.5. GO/TUT/3h

3 hours thiourea treated GO, GO/TUT/3h, was prepared by the same procedure as for GO/TUT/5 min, but in this case, the stirring time at 70°C is 3 hours after addition of 0.67g of thiourea.

2.3.6. GO/TUT/24h

24 hours thiourea treated GO, GO/TUT/24h was prepared by the same procedure as for GO/TUT/5 min, but in this case, the stirring time at 70°C is 24 hours after addition of 0.67g of thiourea.

2.3.7. r-GO

r-GO was prepared by the same procedure as for GO/TUT/5 min, but in this case, the stirring temperature is 80°C and the stirring time after addition of 0.67 g thiourea is 24 hours.

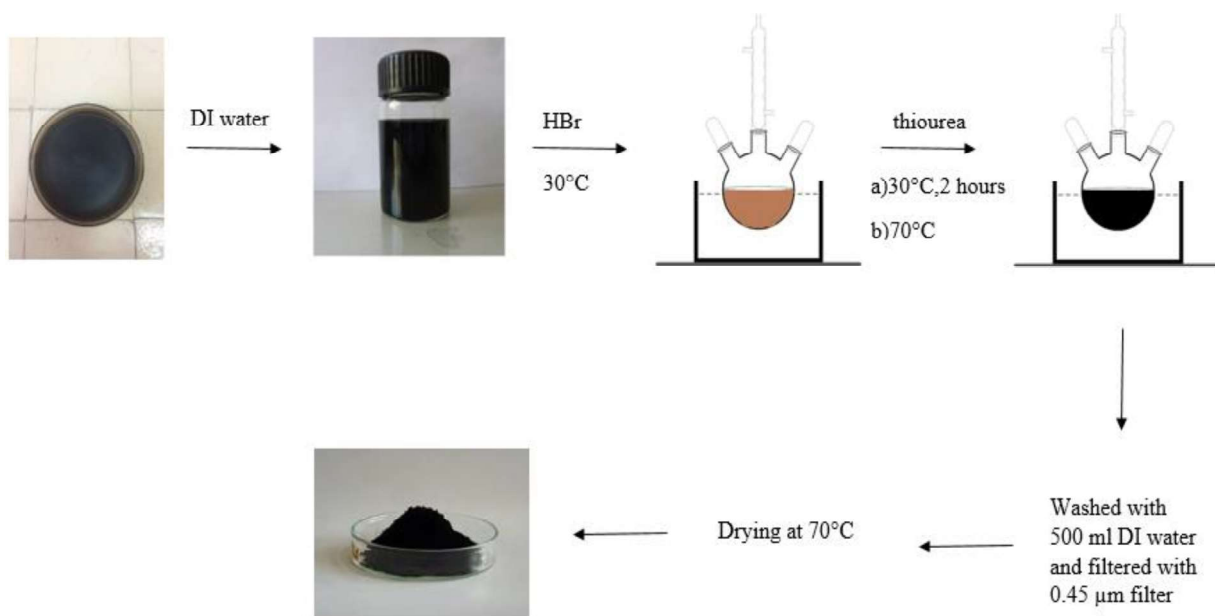


Figure 2.2. Synthesis of thiourea treated graphene oxide materials.

Table 2.1. Samples, exposure time with thiourea and temperature.

Samples	<i>Treatment Time with Thiourea</i>	<i>Temperature (°C)</i>
GO/TUT/5min	5 min	70
GO/TUT/40min	40 min	70
GO/TUT/50min	50 min	70
GO/TUT/60min	60 min	70
GO/TUT/3h	3 hours	70
GO/TUT/24h	24 hours	70
r-GO	24 hours	80

After all samples were dried in an oven, they were put into a schlenk tube, evacuated and placed in liquid nitrogen for 20 minutes. Then, the samples were crashed in a ceramic mortar to obtain a fine powder of GO and GO/TUT samples.

2.4. Characterization of Graphene Oxide

Synthesized GO samples were characterized by Fourier Transform Infrared (FTIR) Spectroscopy (Bruker IFS 66 v/S Vacuum FTIR), X-ray Diffraction (XRD) (Rigaku Miniflex goniometer with X-ray source 30kV/15 mA) and Ultraviolet Visible (UV) Spectroscopy (Hitachi U-2800A Spectrophotometer), Thermogravimetric Analysis (TGA) (Perkin Elmer Simultaneous Thermal Analyzer STA 6000) and Scanning Electron Microscopy (SEM) (Quanta 4000 F Field Emission SEM) techniques.

2.4.1. Fourier Transform Infrared (FTIR) Spectroscopy

Infrared spectroscopy studies on the interaction of infrared light with a material [52]. When molecules are radiated with IR radiation they become excited to various vibrational energy levels [53]. A molecule must undergo a net dipole moment change to absorb IR radiation [53]. This dipole moment change occurs when it vibrates or rotates [53]. Molecules can make electronic transitions when they are radiated with ultraviolet or visible radiation but, they cannot make electronic transitions when they are exposed to IR radiation because IR radiation does not have the enough energy to excite electronic energy levels [53]. Therefore, if the frequency of a given radiation has enough energy to match the natural vibrational frequency of the molecule, it absorbs energy and goes to a higher energy level [53].

IR spectroscopy gives information about the molecular structure of a sample [52]. The absorbance at specific wavelengths of the sample is calculated using the following equation [52]:

$$A = \log \frac{I_0}{I} \quad (2)$$

A = Absorbance,

I_0 = Intensity of the background spectrum,

I = Intensity of the sample spectrum.

Instead of absorbance, percent transmittance (% T) can also be drawn as given in the following equation [52]:

$$\% T = 100 \times \frac{I}{I_0} \quad (3)$$

Infrared spectrum is divided to three parts; far infrared, mid-infrared and near infrared regions [52]. Far infrared region is between $4 - 400 \text{ cm}^{-1}$, mid-infrared region is from between $400 - 4000 \text{ cm}^{-1}$ and near infrared region is between $4000 - 14000 \text{ cm}^{-1}$ [52]. The electromagnetic spectrum showing the regions of infrared is given in Figure 2.1 [52]. As the spectrum goes from right to left, wavenumber, energy and

frequency increases while wavelength decreases since it is inversely proportional with the energy according to the following equation [52]:

$$E = \frac{hc}{\lambda} \quad (1)$$

E = Energy of light (Joules)

h = Planck's constant (Joule-second)

c = Velocity of light (cm/second)

λ = Wavelength (cm^{-1})

Near IR 4000-14000 cm^{-1}	Mid-IR 400-4000 cm^{-1}	Far IR 4-400 cm^{-1}
Molecular vibrations	Molecular vibrations	Molecular vibrations

Figure 2.3. Near, mid and far IR regions.

FTIR consists of the infrared source, interferometer, mirrors and detector [52]. The IR source can be a continuum or monochromatic source [53]. The mostly used IR sources are Nerst Glower, globar, heated nichrome wire, tungsten filament lamp, the CO₂ laser and mercury arc [53]. The commonly used type of interferometer is Michelson interferometer which was first invented by Albert Abraham Michelson [53]. It contains a beamsplitter and colligating mirrors [53]. When the IR beam is emitted from the source, it enters the interferometer and its direction is changed with a mirror and then it comes to the beamsplitter [53]. Beamsplitter is a partially silvered mirror which partially transmits and partially reflects the light [53]. The beamsplitter splits the IR beam into two [53]. One of the beam, travels to the moving mirror and then comes back, while the other one travels to the fixed mirror and comes back. Then, they recombine to form an interference pattern which is read by the detector and given as an IR spectrum in time domain [52,53]. The schematic diagram of IR instrument is given in Figure 2.4.

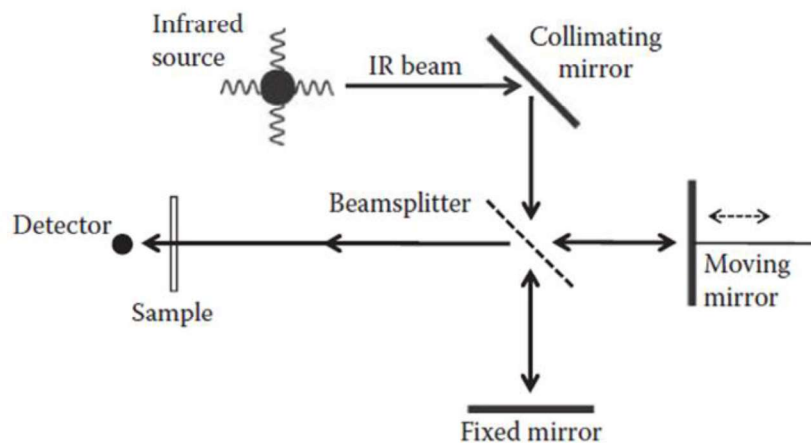


Figure 2.4. Optical diagram FTIR instrument [52].

FT in FTIR corresponds to Fourier transformation and it is a mathematical expression for digital filtering and it is used for converting a signal in time domain to a signal in frequency domain [53]. Fourier transformation was named after French mathematician Joseph Fourier. [52] His theorem shows that many mathematical functions can be expressed as superposition of sine and cosine waves [52]. Today, due to its several advantages, Fourier transformation is preferred in most of the chemical instruments [53]. The first advantage is there are less optical elements and no slit; therefore, the radiant power reaching the detector is higher which gives better signal to noise ratio [53]. The second advantage is wavelength reproducibility and high resolving power which is useful for resolving complex spectra. [53] The third advantage is obtaining whole spectrum of elements in a short time [53].

In this thesis, the FTIR measurements were taken with Bruker IFS 66 v/S Vacuum FTIR instrument with 32 scans at room temperature under vacuum with a resolution of 2cm^{-1} .

FTIR measurements were taken using KBr to prepare pellets and background spectrum was taken with bare KBr pellet. GO samples were mixed with KBr and pellets were prepared using a pressurized press for measuring in FTIR.

2.4.2. X-ray Diffraction (XRD) Analysis

X-ray Diffraction (XRD) spectrometer consist of three main elements, these are X-ray source, sample holder and an X-ray detector [54]. X-rays in the instrument are produced by a source which is a cathode ray tube mostly and have wavelength of approximately 10^{-4} to 10 nm [53,54]. Copper is the most preferred material for this purpose due to giving the shortest wavelength above 1\AA and its high melting point [54,55]. The X-rays come to the monochromator after they are produced from the source and the monochromator filter the X-rays to produce monochromatic X-ray light [54]. Then the sample is scanned by X-rays through a range of 2θ degrees so that all possible diffraction directions will be scanned [54]. In the scanning process, when an X-ray beam strikes the surface of a sample with an angle θ , one part of the beam is scattered by the atoms at the surface [54]. The other part of the beam penetrates to the second layer of atoms and again one part is scattered and one part is penetrated to a third layer of atoms and this goes on as in Figure 2.5 [53]. In Figure 2.5, O, P and R are the atoms in a sample [53]. The X-ray comes with an angle of θ and strikes the surface [53]. If the sum of distances $|AP|$ and $|PC|$ is equal to a fold of the incoming wavelength of the radiation, then the X-ray beam is diffracted [53]. Finally, the reflected X-ray radiation is processed by the detector to give XRD pattern [54]. The schematic diagram of XRD instrument is given in Figure 2.6.

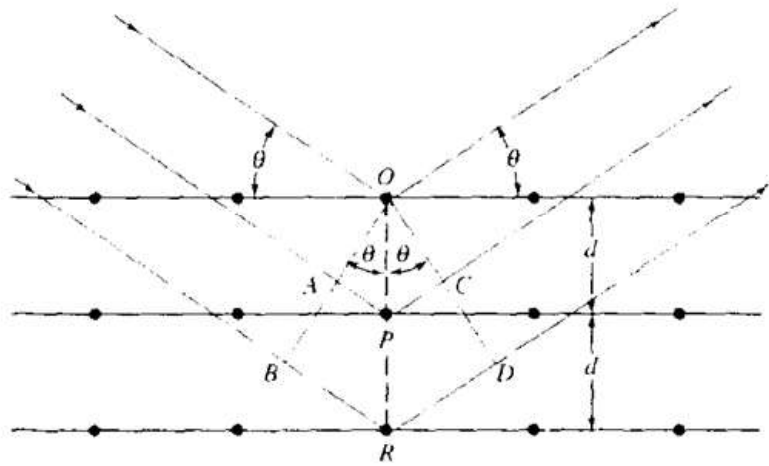


Figure 2.5. X-ray diffraction from a sample [53].

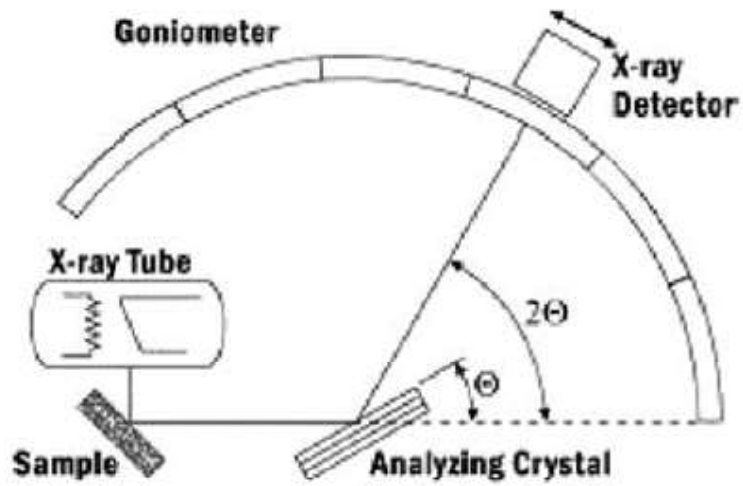


Figure 2.6. Schematic diagram of XRD instrument [54].

In early 1900s, X-rays were defined as particles [54]. On 1912, W. L. Bragg explained the X-rays as waves having the properties of EMR [54]. For atoms to be detected in a sample by X-ray, their spacing must be equal to each other [53]. X-rays' interaction with a sample produces constructive interference when the conditions satisfy the Bragg's Law according to the following equation:

$$d = \frac{n \lambda}{2 \sin \theta} \quad (4)$$

n = an integer,

λ = wavelength of the X-rays (1.54 Å for Cu α X-ray radiation),

d = spacing between the planes (Å), and

θ = diffraction angle.

This formula gives information about the d spacing in a sample by scanning it through 2θ angle in all possible directions. The d spacing of sample is important because it gives information about the characteristics of the sample which are different for all materials [56].

Besides d spacing, using the Debye-Scherrer Equation, the crystalline size of a material can be calculated [57]. The equation is given as:

$$D = \frac{K \lambda}{\beta \cos \theta} \quad (5)$$

D = crystalline size (Å),

K = Scherrer constant (0.89),

λ = wavelength of the X-ray (1.54 Å for Cu α X-ray radiation),

β = full width of half maximum (FWHM) of the peak (in radians) in XRD spectrum, and

θ = diffraction angle.

XRD measurements were taken with Rigaku Miniflex goniometer with X-ray source 30kV/15 mA (Cu K α radiation = 1.54 Å).

2.4.3. Ultraviolet Visible (UV-vis) Spectroscopy

UV-vis spectroscopy is one of the most common techniques to make quantitative and qualitative analysis [53]. The UV-vis spectrophotometer mainly consists of a source, a monochromator, sample compartment and a detector [53]. As a continuum source, hydrogen or deuterium lamps are used [53]. A prism or diffraction grating can be used to isolate the wavelength region to be measured [53]. The sample is irradiated and when radiation is absorbed by the sample, the change in the beam is detected by a detector [53]. The schematic diagram of UV-vis spectrometer is given in Figure 2.7.

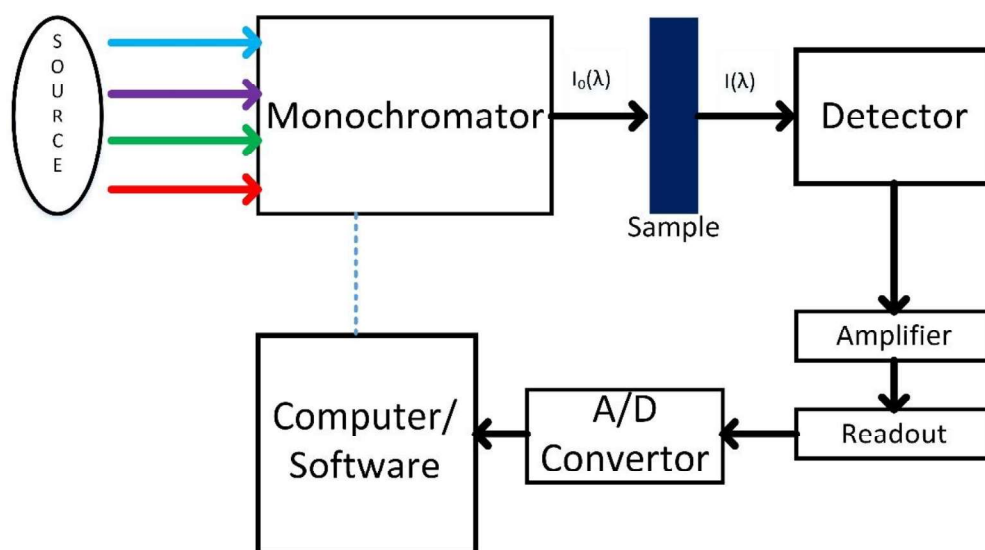


Figure 2.7. Block diagram of UV-vis spectrometer.

A UV-vis spectrometer measures the transmittance or absorbance of a solution [53]. The solution is put into a transparent cell which is made of quartz most of the time. In UV-vis measurements the solvent should be transparent or also it should not give peaks in the region where there are peaks from the sample. Generally, polar solvents like water, alcohols, esters and ketones are used as solvent [53]. The processes after the incident beam strikes the cell wall is seen in Figure 2.8 [53].

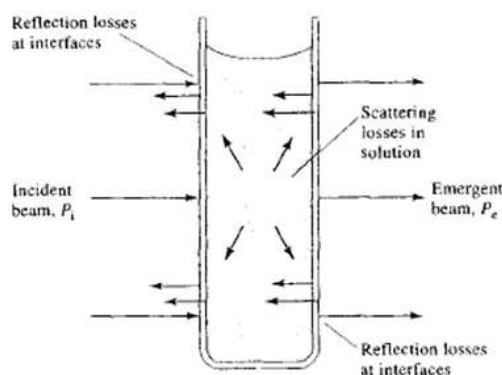


Figure 2.8. Figure showing the reflection and scattering of light in a sample in a transparent cell [53].

When the incident beam (P_i) hits the transparent cell, some of it is reflected and the remaining enters the solution. Some of the entering beam is absorbed by the molecules in the solution and some is scattered [53]. Some of the remaining beam is reflected while leaving the solution [53]. The final beam leaving the cell is P_e and it is measured by the detector. The relation between absorbance and transmittance can be written as [53];

$$A = \log \frac{P_i}{P_e} = -\log T \quad (6)$$

A = absorbance,

P_i = incident light beam power,

P_e = transmitted light beam power, and

T = transmittance

The specific absorptivity constant of a sample can be calculated by using Beer's Law which is given in Equation 7.

$$A = \epsilon b c \quad (7)$$

A = absorbance,

ϵ = molar absorptivity constant ($\text{cm}^{-1} \text{M}^{-1}$),

b = cell path length (cm), and

c = concentration of the sample (M).

The magnitude of the molar absorptivity constant (ϵ) depends on the capture cross section of the sample cell and the probability of a transition to occur by absorbing the incoming light [53]. In this study, the UV-vis measurements were taken with Hitachi U-2800A Spectrophotometer. The sample was put into a quartz cell with 1 cm path length and the UV-vis spectrum was scanned from 200 – 500 nm.

A 0.0100 g of GO was dispersed in 50.0 ml of distilled water in an ultrasonic bath (Bandelin Sonorex RK 100) to make a dispersion with a concentration of 0.2 mg/ml. This is used as a stock solution and desired concentrations were prepared by dilution.

2.4.4. Scanning Electron Microscopy (SEM)

Scanning Electron Microscopy (SEM) which is a type of electron microscopy, was first discovered in 1935 by Knoll [58]. SEM gives detailed information about the surface and the surface morphology of a sample by detection of secondary and backscattered electrons for imaging [53]. It has a higher resolution than light microscopy [58].

The image obtained from the SEM instrument depends on the interaction between the material and the electron beam [59]. The interactions can be divided to two as elastic and inelastic interactions [59]. Elastic scattering occurs when electrons coming from the source hit the specimen surface and scatter without losing energy

with a wide angle [58]. Inelastic scattering occurs when the incident electron beam loses some of its energy to the atom it interacts with [58]. Generally, when the primary beam strikes the surface it does not bound immediately but it penetrates into the sample and collides with the atoms in the sample [58]. The type of this interaction which can be seen in Figure 2.9 depends on the energy of the primary beam and the atomic number [58]. Firstly, if the incident electrons are scattered elastically after interacting with the sample, with an angle more than 90° , they are called as back scattered electrons (BSE) [53,58]. BSE are important for compositional and topographical imaging [53]. They have larger diameter than the primary beam which limits the resolution [53]. Secondly, secondary electrons are produced when the primary beam strikes the surface of the sample and ionizes atoms which are closer to the surface [58]. They have energies less than 50 eV and they give better resolution for topographical imaging [58]. They are used for topographic contrast in SEM images [58]. Thirdly, another result of the interaction of electron beam with sample is X-rays [58]. When the primary electron hits an electron in an inner shell of the sample, another electron from an outer shell will fall in the empty space in the inner shell while emitting X-ray and reestablishing the charge balance [58]. Finally, there are also Auger electrons produced when an electron strikes the sample surface [59]. Auger electrons are produced when the incident electron beam hits an electron from an inner shell and then an outer electron fills the space of the inner electron [59]. These types of electrons are emitted from few nanometers depth of the surface [59].

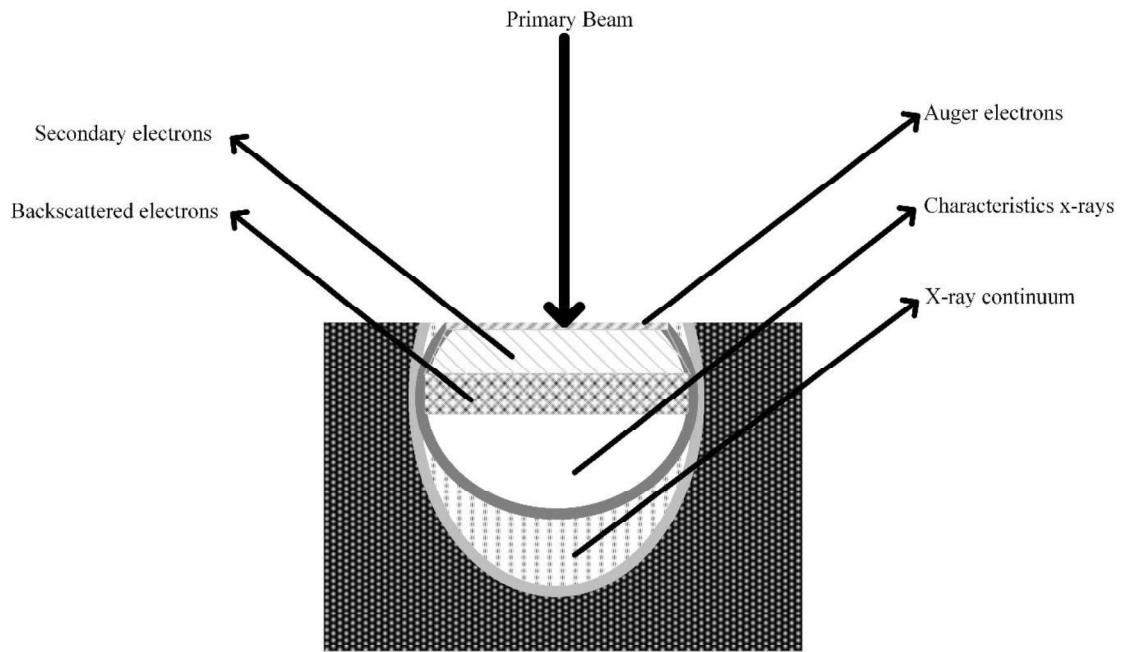


Figure 2.9. Regions showing the electron-sample interaction [53]

The schematic diagram of SEM instrument can be seen in Figure 2.10. The SEM instrument consists of an electron gun which is mostly a tungsten filament source or a field emission gun. The electron gun produces electrons and accelerates them, condenser lenses to focus the electron beam on a specific point, a vacuum environment to prevent scattering of electrons by air, electron beam scanning coils, a stage to put sample and a detector [57].

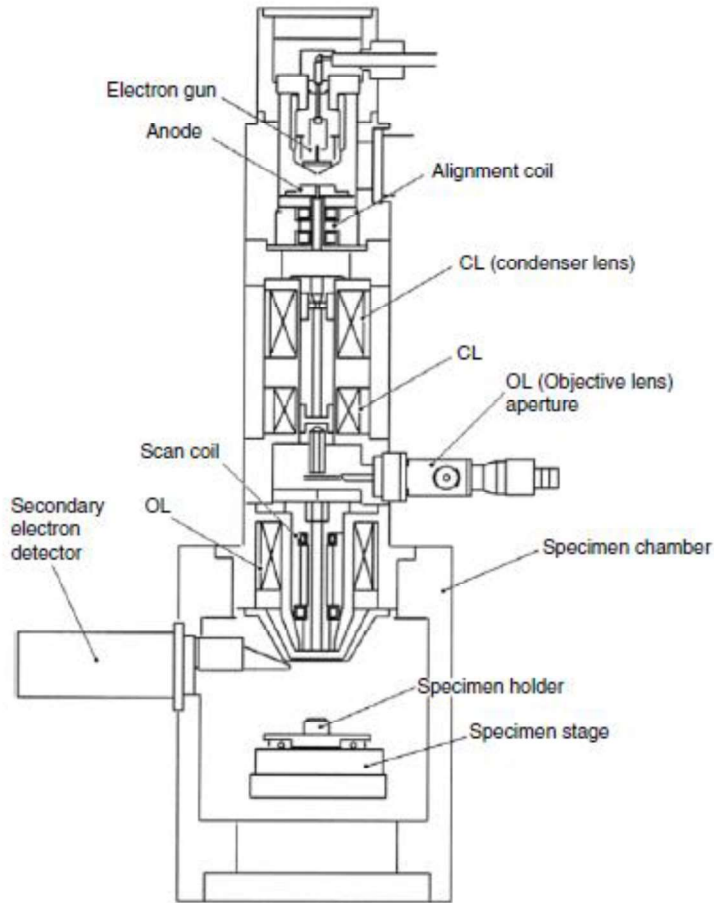


Figure 2.10. Schematic diagram of SEM instrument [57]

The measurements were taken with QUANTA 400F Field Emission SEM instrument. The GO sheet was dispersed in ethanol for 2 hours in an ultrasonic bath (Bandelin Sonorex RK 100). Then, a few milliliters were taken from the dispersion and dropped on to a silicon wafer. The wafer left to dry for an hour and then analyzed with the SEM instrument.

2.5. Thermogravimetric Analysis (TGA)

Thermogravimetric Analysis (TGA) is used for analyzing the weight change of a sample by changing the temperature [60,61]. TGA spectrum is given as changes in the

sample mass in percentage as the temperature is increasing [60]. The measurements are taken in an inert atmosphere under argon, nitrogen or helium gas [62]. TGA measurements can give information about the volatile groups that a sample contains and by knowing the temperature that these groups decompose, information about the groups on the sample can be obtained [62]. The obtained data gives information about the characteristic steps that result with a mass loss of the sample [60].

TGA analysis can be done with very small amount of sample such as 5-10 mg [63]. The sample is weighed in to a ceramic, alumina or platinum crucible [63]. The part where sample is put is called as 'pan' [63]. The sample is heated starting from the desired temperature to a desired higher or lower temperature [62]. The heating happens in the furnace compartment of the instruments [53]. TGA instrument also contains a thermobalance [53]. The balance system works mostly with 'null point' systems [64]. In this systems, a deviation from the mass is detected by a beam [64]. At the starting point equal amount of light is seen from the two photodiodes which is referred as 'null point' [63]. When mass change occurs, different amount of light is seen from the photodiodes and a current is applied to balance again [63]. The amount of current applied is proportional to the lost or gained mass [63].

The TGA measurements were taken with Perkin Elmer Simultaneous Thermal Analyzer STA 6000. The measurements are taken under nitrogen atmosphere and the sample was put in a ceramic crucible.

2.6. Inductively Coupled Plasma Mass (ICP-MS) Spectroscopy

Inductively Coupled Plasma Mass (ICP-MS) Spectroscopy is used for determining the concentration of elements in the sample [53, 68]. Trace elements can be determined by ICP-MS which have low concentration levels [69]. According to IUPAC Gold Book trace element definition is 'Any element having an average concentration less than 100 parts per million atoms' [70]. ICP-MS is a useful technique for detecting trace elements [68]. It can detect parts per billion (ppb) and parts per trillion (ppt) concentrations, therefore, it has high sensitivity [68]. It can be

used in several areas to detect trace elements such as in soil, food, water and biological sample analysis [68].

For ICP-MS analysis both liquid and solid samples can be used but mostly liquid samples are preferred [68]. Liquid sample is introduced by a peristaltic pump. The peristaltic pump, pumps the sample with a speed of approximately 1 ml/min [71]. After the peristaltic pump carries the sample, it is transferred to the nebulizer [71]. The nebulizer converts the liquid sample to aerosol [71]. With the argon gas flow through the chamber, the sample is turned into small droplets and finally fine aerosol [71]. Then the sample goes to the spray chamber [71]. Here, the small sized droplets enter the plasma and the large droplets flow to the waste compartment [71].

The plasma in ICP-MS instrument is generated in the torch which is mostly made of quartz [68]. The torch contains a quartz tube and a copper coil surrounded on the end of this tube [68]. Radio frequency (RF) goes through the coil while the argon gas is pumped from the tube to the torch [68]. A spark is generated first and this ionizes an argon atom and generate an electron. By collision more electrons are generated and they accelerate and fluctuate through magnetic field generating the plasma [53]. After sample is carried, the ions will collide with argon atoms and further ionize increasing the temperature [53]. The temperature of the plasma is between 6000-10 000 K [68]. The part where plasma is generated is in atmospheric pressure while the mass spectrometer is at a vacuum of 10^{-6} torr [68]. Due to this pressure difference an interface section is required in ICP-MS to prevent electrical discharge between plasma and the coil [68]. After the interface part, the ions directed to the mass spectrometer part [68]. The mass spectrometer gives information using mass to charge (m/z) ratio [53]. The most of the mass spectrometers contain a quadrupole [68]. Quadrupole consists of four rods, two of them have positive voltage and two of them have negative voltages [68]. The ions move through the quadrupole while Direct Current (DC) and Rf frequency Alternating Current (AC) voltages are applied to the rods [71]. The ions which have different m/z ratios diffract from the path in the quadrupole [71]. Therefore, the ions which have specified m/z ratios are detected by the detector [71].

The schematic diagram of ICP-MS instrument is given in Figure 2.11. The ICP-MS measurements were taken with Thermo Fischer X Series ICP-MS instrument.

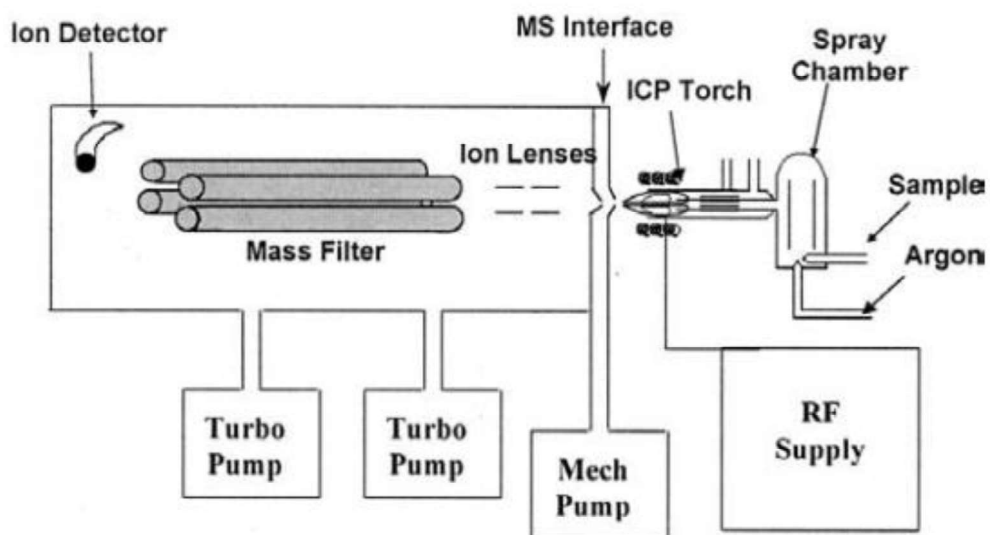


Figure 2.11. Schematic diagram of ICP-MS instrument [70].

2.6.1. Preparation of Stock Pb^{+2} Solution

0.5 ml of concentrated HNO_3 (65%) solution was diluted to exactly 50.0 ml in a falcon tube to prepare 1% (v/v) HNO_3 solution. Then, exactly 0.80 g of $\text{Pb}(\text{NO}_3)_2$ was dissolved in 1% HNO_3 solution. Finally, 10 000 ppm Pb^{+2} stock solution was prepared. The $\text{Pb}(\text{NO}_3)_2$ solid was dissolved according to the following equation;



From this stock solution, the standard solutions were prepared by doing serial dilutions.

2.6.2. Preparation of Standard Samples

The standard solutions were directly prepared from 10 000 ppm Pb^{+2} stock solution by external standard method. Standard solutions with concentrations 10, 20, 40 and 75 ppb were prepared by taking 0.05 ml, 0.1 ml, 0.2 ml and 0.375 ml from stock solution and diluted with 1% HNO_3 exactly to 50.0 ml, respectively.

2.6.3. Sample Preparation for Pb^{+2} Adsorption on GO According to Time

50 ppm Pb^{+2} solution was prepared from the 10 000 ppm Pb^{+2} stock solution by taking 0.25 ml from stock solution and diluting to exactly 25.0 ml by DI water. Then, 10.0 mg GO sample was weighed and put into 25.0 ml of 50 ppm Pb^{+2} solution. 5 different samples were prepared for measuring the adsorption capacity of GO depending on treatment time as 10 min, 20 min, 30 min, 50 min and 60 min. The samples were stirred on a mechanic stirrer at 150 rpm at room temperature. Then, they were classified according to the stirring time. Afterwards, they were filtered with Chima Blue Ribbon filter paper with pore size smaller than 2 μm . The remaining Pb^{+2} left in the supernatant was collected and the filter paper washed with additional 25.0 ml DI water. Then, the collected 50.0 ml sample was analyzed with ICP-MS instrument.

2.6.4. Sample Preparation for Adsorption Capacity of GO with Different Concentrations of Pb^{+2} Solutions

In order to find the maximum adsorption capacity of GO, different concentrations of Pb^{+2} solutions were prepared. To find the unknown concentrations of GO solutions, standard solutions which were prepared as 10 ppb, 20 ppb, 40 ppb and 75 ppb were used to draw a calibration curve. The concentrations of the prepared GO solutions are 25 ppm, 100 ppm, 250 ppm, 500 ppm, 750 ppm, 1000 ppm and 1500 ppm. The solutions were prepared from 10 000 ppm stock Pb^{+2} solution. Respectively

62.5 μL , 250 μL , 625 μL , 1.25 ml, 1.875 ml, 2.5 ml and 3.75 ml were taken from 10 000 ppm Pb^{+2} stock solution and diluted to 25.0 ml. Then, approximately 10 mg of GO was added to the solution and mixed at room temperature on mechanical stirrer for 1 hour. After stirring, the solutions were filtered with Chima Blue Ribbon filter paper with pore size smaller than 2 μm and washed with additional 25.0 ml DI water to get 50.0 ml solution. The unadsorbed Pb^{+2} concentration left in the solution was measured by ICP-MS.

2.6.5. Sample Preparation for Pb^{+2} Adsorption on GO/TUT Samples

The Pb^{+2} adsorption capacities of GO/TUT samples were measured for comparing their capacity with GO. To find the unknown concentration of samples, first standard solutions were prepared from 10 000 ppm Pb^{+2} stock solution. From stock solution, 1 ppm solution was prepared which was used for preparing the standard solutions with concentrations 10 ppb, 20 ppb, 40 ppb and 75 ppb. Then, from the 10 000 ppm stock solution, 1000 ppm solutions were prepared by taking 2.5 ml and diluting to 25.0 ml. Approximately 10 mg of GO/TUT compounds were put into the solutions and mixed at room temperature on mechanical stirrer for 1 hour. Then, the solutions were filtered with Chima Blue Ribbon filter paper with pore size smaller than 2 μm and washed with 25.0 ml DI water to make 50.0 ml solutions. The solutions containing unadsorbed Pb^{+2} were analyzed with ICP-MS.

CHAPTER 3

RESULTS AND DISCUSSION

In this study, GO, GO/TUT/5min, GO/TUT/40min, GO/TUT/50min, GO/TUT/60min, GO/TUT/3h, GO/TUT/24h and r-GO samples were prepared, characterized and used for adsorption of Pb^{+2} ion in aqueous solutions. The synthesized samples for this study are given in Table 3.1. The characterization of the synthesized materials was performed with FTIR, XRD, SEM and TGA. Finally, Pb^{+2} adsorption capacities of these materials were determined by ICP-MS.

Table 3.1. *Samples, treatment time with thiourea and temperature.*

Samples	<i>Treatment Time with Thiourea</i>	<i>Temperature (°C)</i>
GO	-	-
GO/TUT/5min	5 min	70
GO/TUT/40min	40 min	70
GO/TUT/50min	50 min	70
GO/TUT/60min	60 min	70
GO/TUT/3h	3 hours	70
GO/TUT/24h	24 hours	70
r-GO	24 hours	80

3.1. Characterization of Graphene Oxide

As it is well known that graphene has a honeycomb structure consisting of very strong C-C bonds with sp^2 hybridization [34]. Due to these strong C-C bonds and hydrophobicity of graphene, it is difficult to use graphene for adsorption studies of heavy metals from aqueous solutions [34]. Therefore, strong acids such as H_2SO_4 and/or HNO_3 and/or H_3PO_4 , and an oxidizing agent such as $KMnO_4$ or $KClO_3$ can be used to functionalize the surface of graphene by carbonyl, carboxyl, hydroxyl and epoxide groups, which makes it hydrophilic [41]. The proposed structure of GO is given in Figure 3.1. In this work H_2SO_4 , H_3PO_4 and $KMnO_4$ were used for the synthesis of GO and it was synthesized by FTIR, UV-vis, XRD, SEM and TGA techniques.

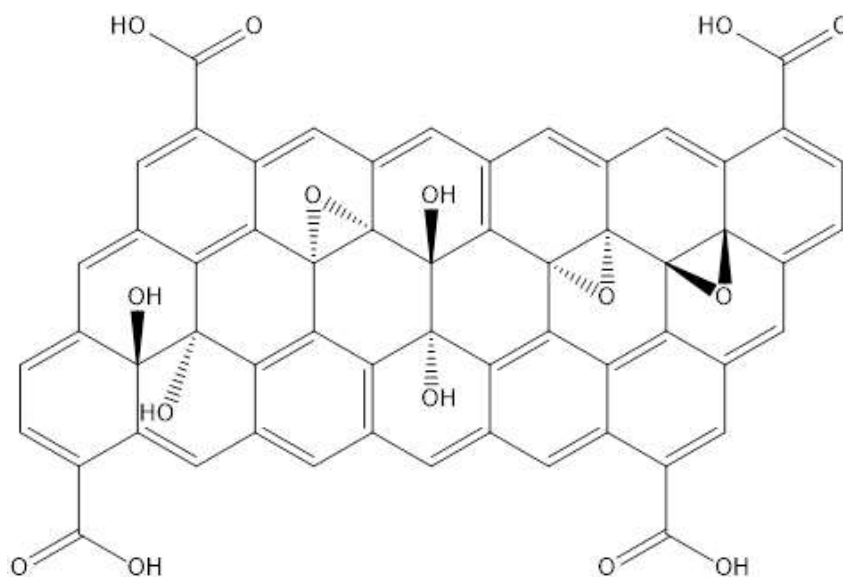


Figure 3.1. Representative structure of GO [38,87]

3.1.1. FTIR Spectrum of GO

The FTIR spectrum of GO gives information about the structure of GO by showing specific functional groups and backbone structure of GO. The FTIR spectrum of GO is given in Figure 3.2. As can be seen from the figure, a broad peak is observed at 3435 cm^{-1} originates from O-H stretching [41]. The peak at 1740 cm^{-1} and 1625 cm^{-1} correspond to C=O in carboxylic acid and/or carbonyl moieties [41], and vibration of unoxidized graphitic C=C, respectively [41]. It is believed that the peak at 1388 cm^{-1} might be due to C-OH deformation and/or carbonyl group [41] and the peaks at 1221 and 1050 cm^{-1} might arise from C-O-C stretching of epoxy and C-O of alkoxy groups, respectively [41]. It is reported that the peak at 590 cm^{-1} might be owing to C-H wagging [41].

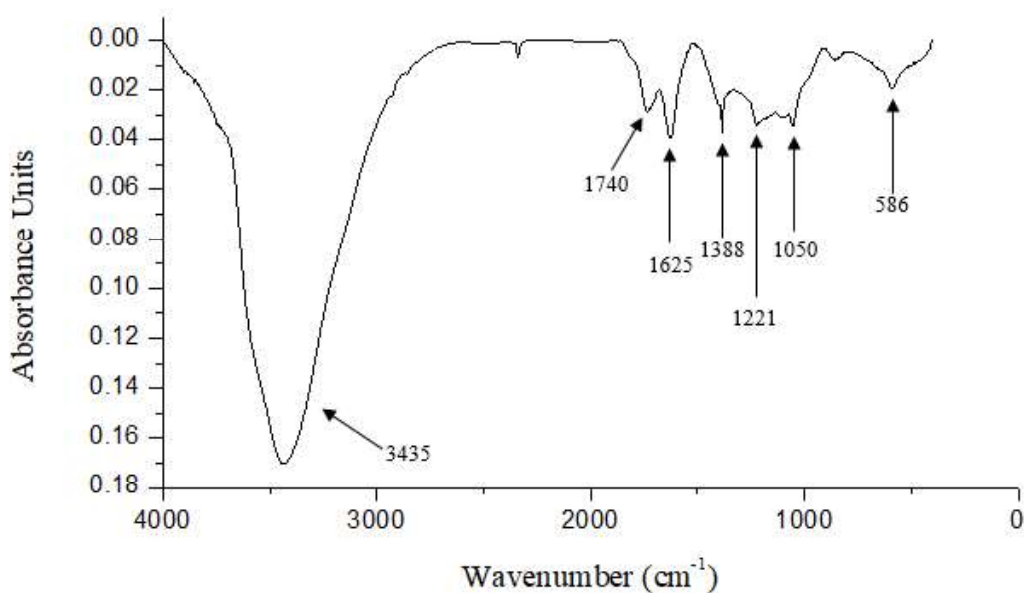


Figure 3.2. FTIR spectrum of GO

There are several studies interpreting the FTIR spectrum of GO and summary of these studies in the literature are given in Table 3.2. According to the results, $3000\text{-}3600\text{ cm}^{-1}$ shows OH, $1720\text{-}1740\text{ cm}^{-1}$ indicates carbonyl (C=O) of carboxyl group and/or carbonyl moieties, $1590\text{-}1625\text{ cm}^{-1}$ demonstrates unoxidized C=C in graphite domain and/or adsorbed H₂O, $1380\text{-}1418\text{ cm}^{-1}$ displays C-OH deformation or

carboxyl group or OH, 1050 and 1226-1250 cm^{-1} reveals epoxide and 1049-1080 cm^{-1} point out alkoxy groups [41,72-79].

Table 3.2. Table showing mid- IR vibrations of functional groups

OH	C=O of carboxyl groups and/or carbonyl moiety	C=C of unoxidized graphite or adsorbed H ₂ O	C-OH deformation or carbonyl group or OH	Epoxy	Alkoxy	References
3435	1740	1625	1388	1221	1050	our results
3420	1720-1740	1590-1620	-	1250	-	41
3407	1731		1401	1228	1080	72
3405	1727	1621	1403	1224	1049	73
3425	1734	1621	1410	1230	1050	74
	1734	1624	1415	1228	1076	75
3000-3600	1730	1620	-	-	1039	76
3432	1736	-	-	1227 and 988	-	77
-	1734	-	1418	1226	1052	78
3200	1718	1600	1380	1050	-	79

3.1.2. UV-vis Spectrum of GO

UV-VIS spectrum of GO is given in Figure 3.3. A typical π to π^* transition in C=C was observed at 222 nm as given in the literature [41, 80]. In addition, the absorptivity constant of GO was calculated by using Beer's Law as $A=\epsilon bc$. In the formula, A is absorbance, ϵ is the absorptivity constant ($\text{cm}^{-1} \text{M}^{-1}$), b is the cell path length (cm) and c is the concentration (M). The absorptivity constant (a) was found as $(4.31 \pm 0.11) \times 10^4$ (2.72%) ml/mg.m. Su et al. studied the absorption coefficient for GO synthesized from different type of graphite flakes and found results between 2.67×10^6 and 6.72×10^6 ml/mg.m [81]. Coleman et al. reported the absorption coefficient for GO as 1390-6600 ml/mg.m [81]. The difference in the absorptivity constant of GO

might be due to the differences in the preparation method or the solubility of GO in DI water [81].

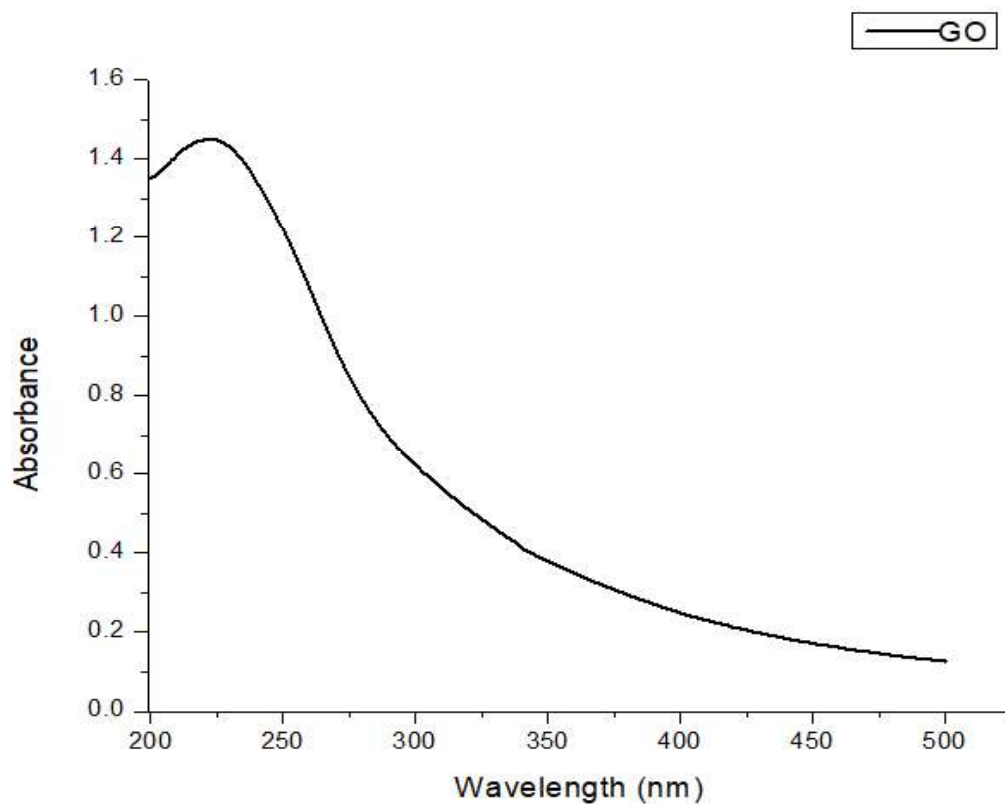


Figure 3.3. UV-vis spectrum of GO

3.1.3. XRD Spectrum of GO

The XRD pattern is used to define the crystalline size, number of layers and distance between the layers of GO. The XRD pattern of GO is given in Figure 3.4. It consists of one sharp peak, $2\theta=12.36^\circ$, corresponds to the 100 plane of GO and one broad peak, $2\theta=23.54^\circ$, originates from 002 plane of unoxidized graphene left in the sample.

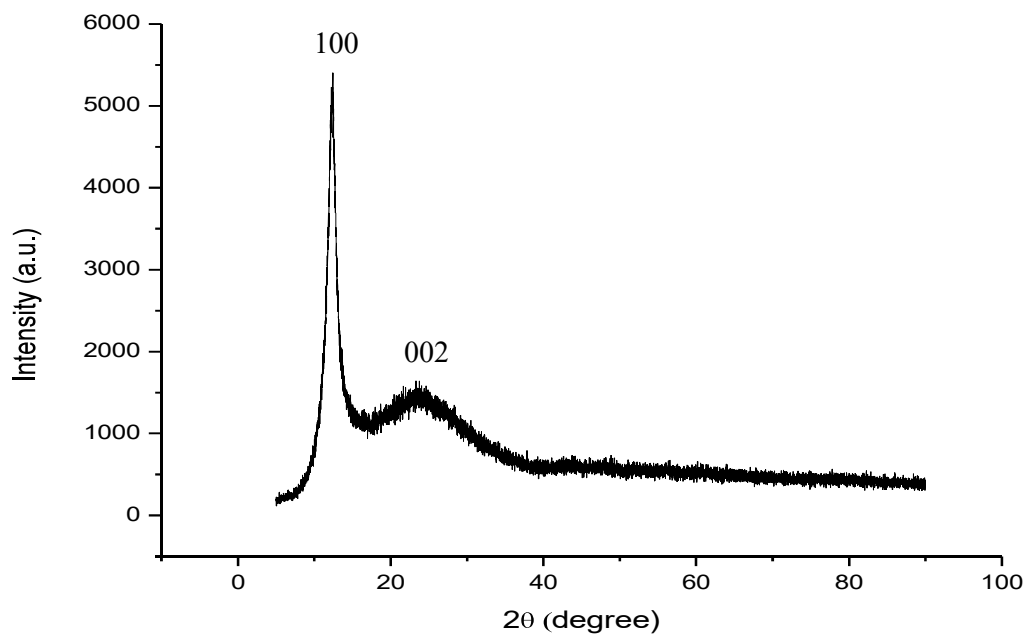


Figure 3.4. XRD spectrum of GO

The distance between the layers known as ‘interlayer spacing’ (d) was calculated by Bragg’s Equation, given below, and it was found that the distance between the 100 and 002 layers of GO are 7.15 Å and 3.77 Å, respectively.

$$d = \frac{n \lambda}{2 \sin \theta} \qquad \text{Bragg's Equation}$$

n = an integer,

λ = wavelength of the x-rays (1.54 Å for Cu α x-ray radiation),

d = spacing between the planes (Å), and

θ = diffraction angle.

For 2θ=12.36° peak (100 plane) the interlayer spacing is,

$$d = \frac{1 \times 1.54 \text{ \AA}}{2 \sin 6.18} = 7.15 \text{ \AA}$$

For $2\theta=23.54^\circ$ peak (002 plane) the interlayer spacing is,

$$d = \frac{1 \times 1.54 \text{ \AA}}{2 \sin 11.77} = 3.77 \text{ \AA}$$

As stressed above, small interlayer distance, which is close to graphite (3.35 Å) is due to unoxidized graphene left in the sample. The large interlayer spacing indicates an insertion of oxygen containing functional groups between the layers, as expected [41].

In addition to interlayer spacing, the crystalline size of GO was also calculated using Debye-Scherrer Equation, given below, and found to be 47.26 Å and 6.55 Å for 100 and 002 planes, respectively.

$$D = \frac{K \lambda}{\beta \cos\theta} \quad \text{Debye-Scherrer Equation}$$

D = crystalline size (Å),

K = Scherrer constant (0.89),

λ = wavelength of the X-ray (1.54 Å for Cu α X-ray radiation),

β = full width of half maximum (FWHM) of the peak (in radians) in XRD spectrum,
and

θ = diffraction angle.

For $2\theta=12.36^\circ$ peak (100 plane) crystalline size is,

$$D = \frac{0.89 \times 1.54 \text{ \AA}}{0.0281 \times \cos(6.18)} = 47.26 \text{ \AA}$$

For $2\theta=23.54^\circ$ peak (002 plane) crystalline size is,

$$D = \frac{0.89 \times 1.54 \text{ \AA}}{0.02138 \times \cos(11.77)} = 6.55 \text{ \AA}$$

It is possible to calculate the number of layers by taking the ratio of crystalline size to interlayer spacing:

$$\text{No of layers} = \frac{\text{crystalline size}}{\text{interlayer spacing}}$$

$$\frac{D}{d} = \frac{47.26 \text{ \AA}}{7.15 \text{ \AA}} = 6.61 \text{ layers for (100) plane}$$

$$\frac{D}{d} = \frac{6.55 \text{ \AA}}{3.77 \text{ \AA}} = 1.74 \text{ layers for (002) plane}$$

It was interesting to observe staking of larger number of layers for GO compared to unoxidized graphene. Table 3.3 shows the summary of calculated results for the XRD plot of GO.

Table 3.3. *Interlayer spacing, crystalline size and number of layers for GO*

Plane	Peak Position	d	D	D/d
100	12.36°	7.15 Å	47.26 Å	6.61 layers
002	23.54°	3.77 Å	6.55 Å	1.74 layers

There are several studies in the literature that reveal the XRD pattern of GO. These studies are summarized in Table 3.4. As can be seen from the table, GO has much higher interlayer spacing than r-GO or graphene due to the functional groups on the surface of GO [82-85].

Table 3.4. XRD measurement results in the literature

GO	Unoxidized graphene and/or r-GO	Graphite (sharp peak)	Reference
12.36° (d=7.15Å)	23.54° (d=3.63Å)	-	Our results
10.10° (d=8.75Å)	24.10° (d=3.68Å)	26.38 (d= 3.35Å)	82
11.90° (d=7.40Å)	-	26.70° (d=3.30Å)	83
9.98° (d=9.00 Å)	23.79° (d=4.00Å)	26.50° (d=3.36 Å)	84
11.12° (d=8.10Å)	25.50° (d=3.50Å)	26.60° (d=3.40Å)	85

3.1.4. SEM Images of GO

The SEM images of GO are given in Figures 3.5. From the SEM images the GO sheets can be seen clearly. However, each layer cannot be distinguished from the whole structure. Therefore, to find the number of layers of GO, XRD has given better information.

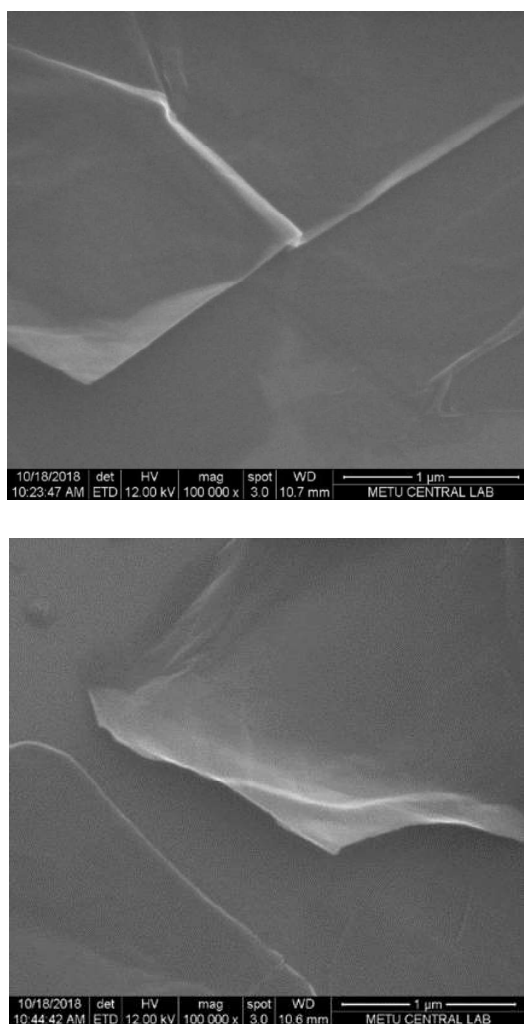


Figure 3.5. SEM images of GO

3.2. Characterization of Thiourea Treated GO Materials

The thiourea treated GO materials were analyzed by FTIR and XRD spectroscopy techniques.

3.2.1. FTIR Spectrum of GO/TUT Materials

In order to decide the time for thiourea treatment, the reaction was followed by taking small amount of sample from the reaction medium for different time, for instance, 5 min., 10 min, 20 min., 30 min., 40 min., 50 min., 60 min., 75 min., 90 min., 105 min., 120 min., 150 min., 3 hours, 4 hours, 4.5 hours, 5 hours, 24 hours at 70°C and 24 hours at 80°C. The results are given in Figure 3.6. For comparison, thiourea and GO spectra are also added to the figure. As can be seen from the figure, the major changes in the spectrum were noticed at 5 min., 40 min., 50 min., 60 min., 3 h, 24 h at 70°C and 80° (r-GO). Therefore, these time intervals were chosen for the preparation of the sample and named as GO/TUT/5min, GO/TUT/40min, GO/TUT/50min, GO/TUT/60min, GO/TUT/3h, GO/TUT/24h and r-GO.

FTIR spectrum of thiourea, revealed typical peaks at 1589 cm^{-1} ($\delta(\text{NH}_2)$), 1469 cm^{-1} ($\gamma(\text{N-C-N})$), 1099 cm^{-1} ($\gamma(\text{N-C-N}) + \delta(\text{NH}_2) + \gamma(\text{C=S})$), 725 cm^{-1} ($\gamma(\text{C=S}) + \gamma(\text{N-C-N})$), 624 cm^{-1} ($\beta(\text{S=C-N})$) and 503 cm^{-1} ($\delta(\text{N-C-N})$). GO spectrum's interpretation was given in the previous section [86]. It is obvious that any of the FTIR spectra of thiourea treated GO do not resemble the thiourea and GO itself. They are totally different and have specific peaks at certain positions, Figure 3.7. This might be due to the attachment of thiourea on the surface of GO. The proposed thiourea attachment is given by W. S. V. Lee et al and shown in Figure 3.8 [87]. As can be seen from the figure, N or S atoms of thiourea attached to the carbonyl functional group of the GO.

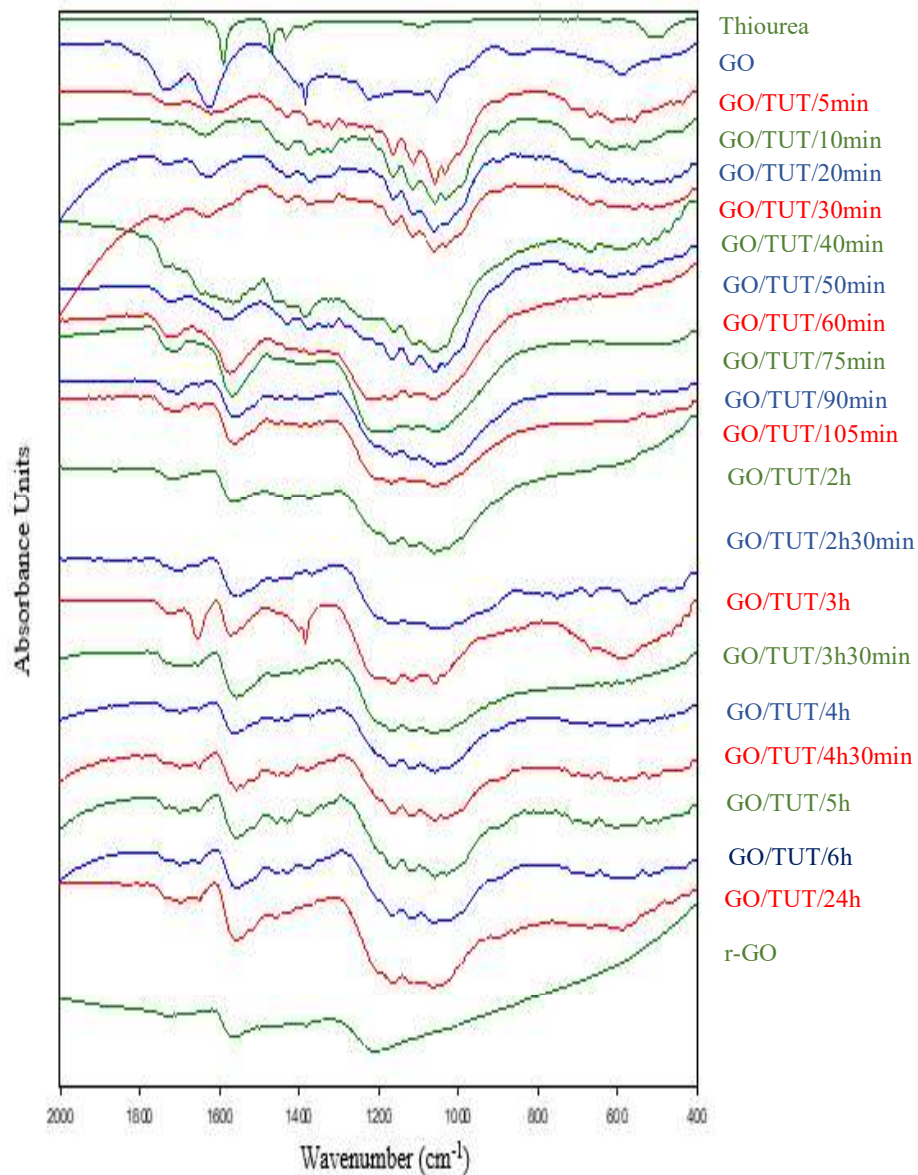


Figure 3.6. FTIR spectrum of GO/TUT materials with respect to treatment time with thiourea

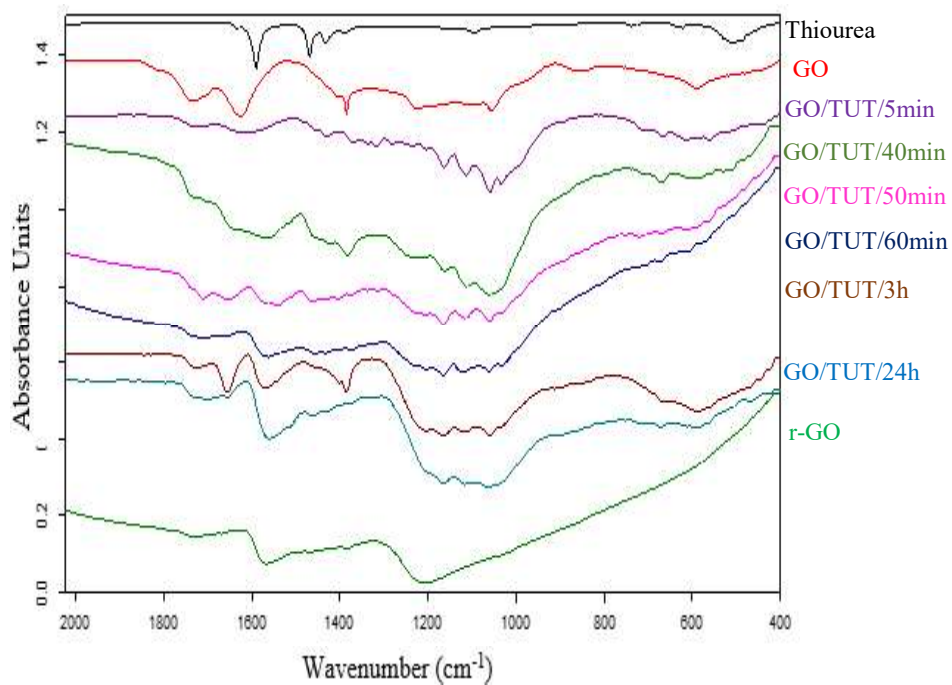


Figure 3.7. FTIR spectrum of selected GO/TUT samples with thiourea

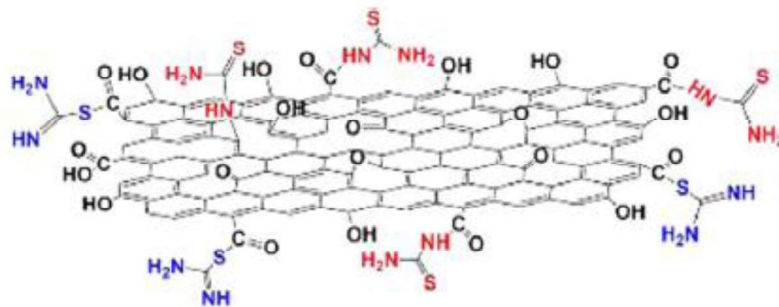


Figure 3.8. Thiourea functionalized GO structure [87]

In addition to the carbonyl groups, thiourea can be attached to the epoxide and hydroxyl groups of GO such as Chua et al. proposed [43]. In their study, they

synthesized thiol functionalized GO by treating GO first with HBr, then thiourea and finally by NaOH [43]. In our study, GO was also treated with HBr to brominate the hydroxyl and epoxide groups on GO. HBr is preferred because Br is a good leaving group. The bromination causes the opening of epoxide group and the oxygen atoms of epoxide and hydroxyl groups leave while Br atom binds to the empty carbon atom. When thiourea is added it binds to the bromine moieties, then Br atom leaves by forming isothiuronium salts on the surface of the sample [43]. The mechanism is in Figure 3.9.

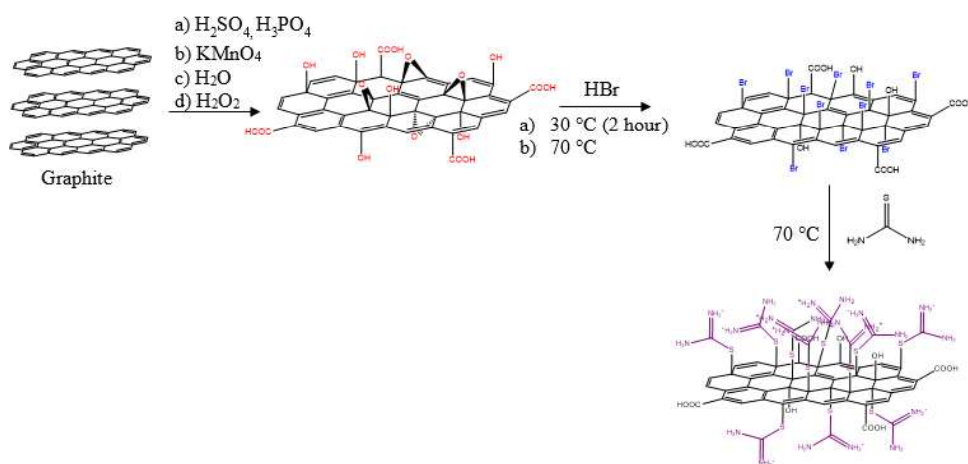


Figure 3.9. Mechanism of thiourea attachment on GO [43]

3.2.2. XRD Spectrum of GO/TUT Materials

XRD pattern of GO and thiourea treated GO are given in Figure 3.10. As can be noticed from the figure, a characteristic GO peak at 12.36° is disappeared and very broad peaks are observed at approximately 22° . The interlayer spacing, crystalline size and number of layers were calculated for all samples and it was found that the interlayer spacing is the largest for GO (7.15 \AA), smallest for r-GO (3.87 \AA) due to removing of oxygen containing functional groups attached to the GO surface and it is

approximately 4.0 Å for GO/TUT samples. In addition to these, the largest number of layers were observed for GO and smallest for GO/TUT/5min, indicating that GO/TUT/5min was almost completely exfoliated to individual layers and did not restack. The other samples have number of layers between 2-3 layers. These data are summarized in Table 3.5.

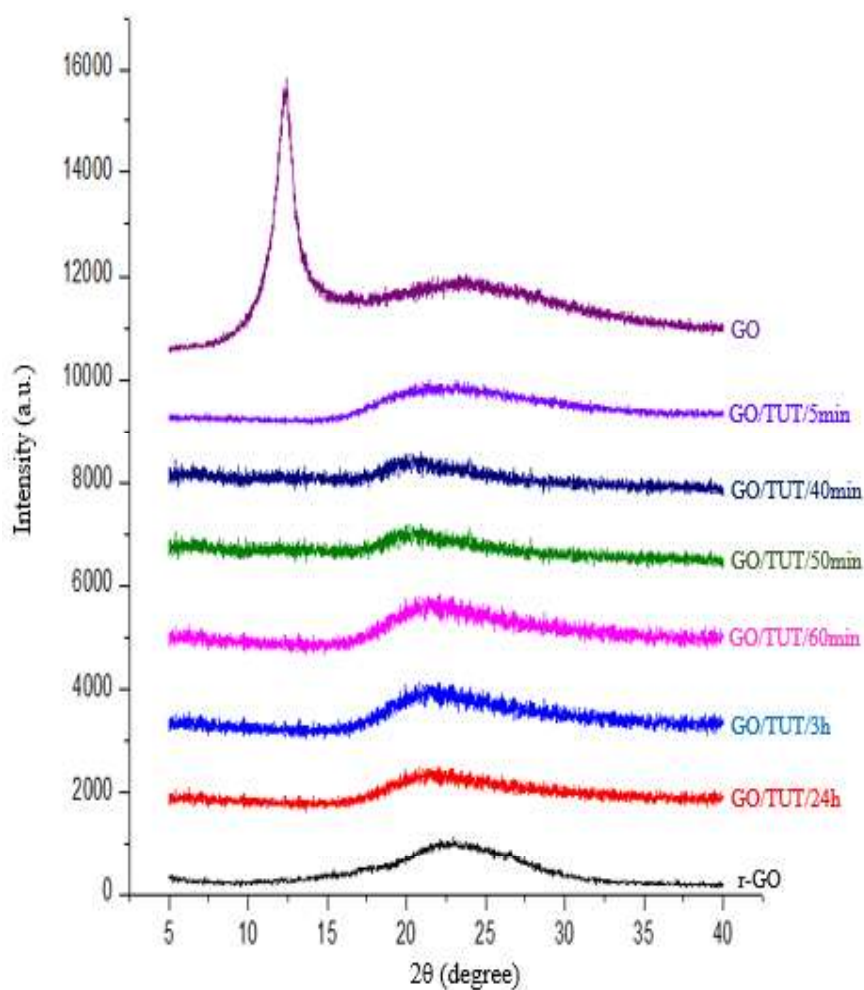


Figure 3.10. XRD pattern of GO and GO/TUT materials

Table 3.5. Interlayer distance, crystalline size and number of layers of GO samples

Sample	$2\theta(^{\circ})$	FWHM (radian)	Interlayer spacing (\AA)	Crystalline size (\AA)	Number of layers
GO	12.36	0.0281	7.15	47.26	6.60
GO/TUT/5min	22.6	0.2926	3.93	4.78	1.22
GO/TUT/40min	20.85	0.1837	4.25	7.76	1.83
GO/TUT/50min	20.42	0,1009	4.34	13.79	3.18
GO/TUT/60min	21.46	0.1411	4.14	9.26	2.24
GO/TUT/3h	21.50	0.1312	4.13	10.63	2.57
GO/TUT/24h	21.55	0.1426	4.12	9.71	2.35
r-GO	22.92	0,1321	3.87	10.59	2.73

3.3. Thermal Gravimetric Analysis (TGA) Measurements

Thermal stability studies of samples were achieved by Thermal Gravimetric Analysis (TGA) measurements and all graphs are given in Figure 3.10, 3.11, 3.12 and 3.13. In order to show the results clearly, the TGA graphs of the samples are given in different figures.

It is obvious from Figure 3.10 that there is not much weight loss for graphite itself, indicating that it is the most stable sample among the others until 700°C. The r-GO also revealed good thermal stability compared to GO. Only 3% weight loss was observed due to adsorbed H₂O [65] and gradual weight loss (22%) was obtained between 100-700°C, due to decomposition of residual organic functional groups on graphene sheets, indicating an efficient removal of oxygen containing functional groups after reduction process.

TGA of GO showed four weight loss steps with increase in temperature as seen clearly in Figure 3.11a and 3.11b. In the first step, 17% weight loss was detected between 30-100°C, which can be attributed to the removal of moisture, in the second step, sudden weight loss (25%) was noticed between 150-180°C, which assigned to

decomposition of labile oxygen containing functional groups, third and fourth weight losses were discerned between 200-350°C and 350-700°C, respectively, which might be due to degradation of remaining functional groups.

For comparison, TGA of thiourea itself is also given in Figure 3.11. As can be seen from the figure, there is an abrupt weight loss (90%) between 200-250°C due to decomposition of thiourea, and it is the least stable species after approximately 220°C compared to the others. Similar trend was observed for TGA of GO and GO/TUT/5min, but GO/TUT/5min is more stable than GO as seen in Figure 3.12. 5% weight loss was detected for GO/TUT/24h between 30-100°C due to adsorbed H₂O as given before [65], and sudden weight loss (~37%) was noted between 150-320°C which can be ascribed to the decomposition of oxygen and/or sulfur and/or nitrogen containing functional groups are given in Figure 3.12. TGA trend for the other GO/TUT samples are quite similar, first weight loss was obtained for adsorbed H₂O and then for functional groups adsorbed on the surface of materials as seen clearly in Figure 3.13.

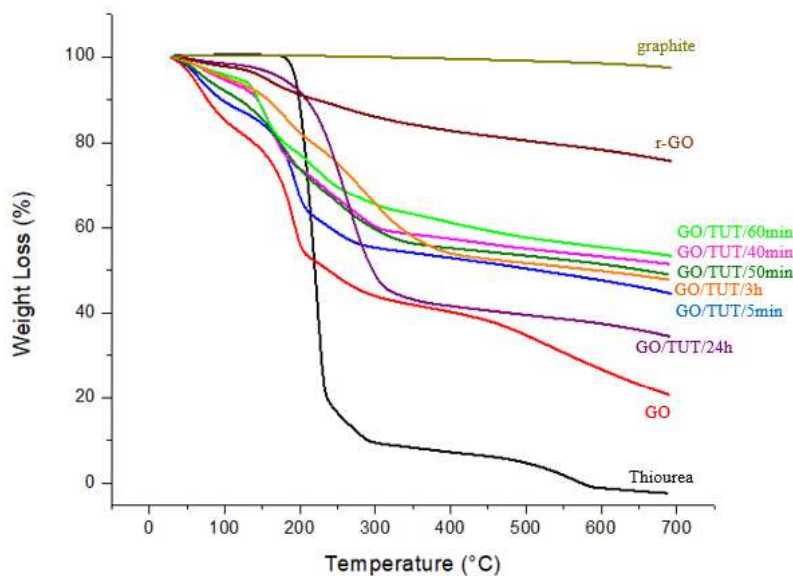


Figure 3.10. TGA plot of GO samples, thiourea and graphite.

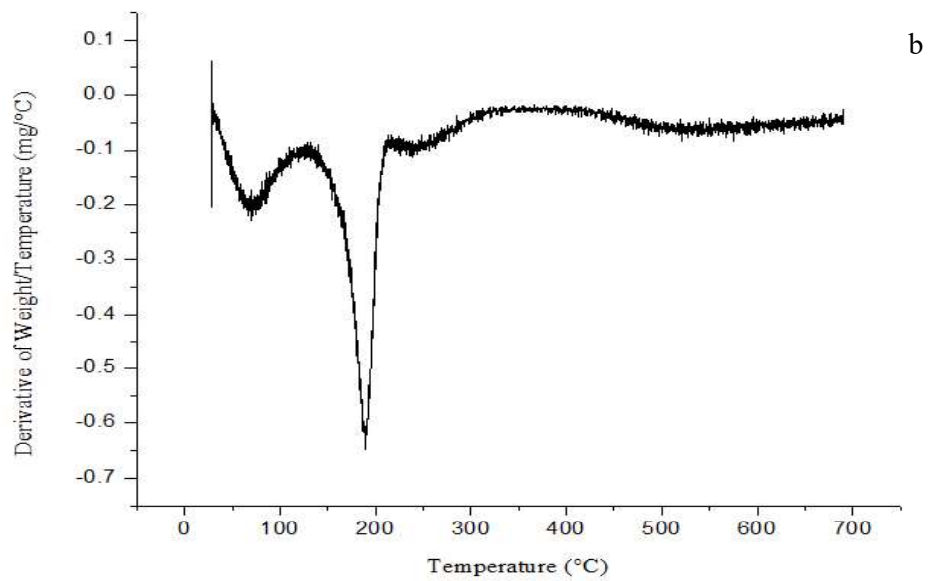
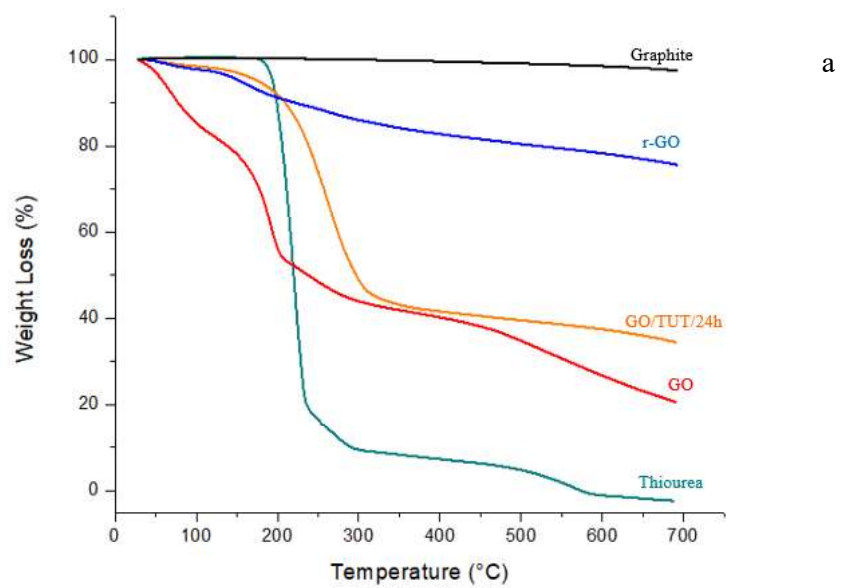


Figure 3.11. a) TGA plot of graphite, r-GO, GO/TUT/24h, GO and thiourea, b) Differential thermal analysis plot of GO.

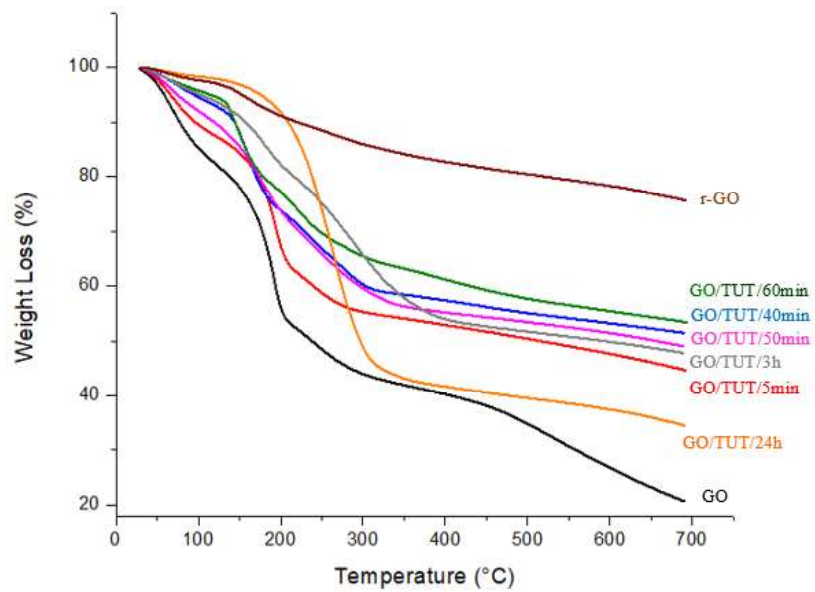


Figure 3.12. TGA plot of GO/TUT samples, GO.

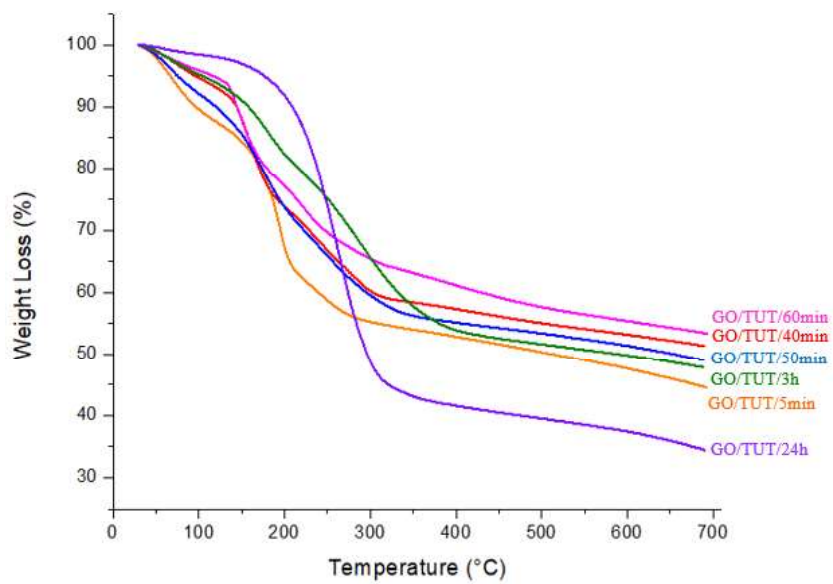


Figure 3.13. TGA plot of GO/TUT samples treated at 70°C.

3.4. ICP-MS Measurements

Using ICP-MS, the Pb^{+2} adsorption capacity of the samples were measured. To control the signal intensity of ICP-MS a known concentration solution, Tune A, is first introduced to the instrument. Tune A contains Pb(II), Li(I), In(II), Co(II), U(IV) and Bi(V) elements with concentration of 10 ppb. After controlling the signal intensity of ICP-MS, the standards and the solutions were introduced into the plasma. The instrument gives the data as counts per second (cps) and it is converted to concentration by using the calibration curve drawn by standard solutions. In this study, the concentration of Pb^{+2} was measured from standard solutions and unknown samples of GO and GO/TUT samples. The Pb^{+2} stock solution which was prepared from $\text{Pb}(\text{NO}_3)_2$ used for preparing the standard solutions having concentrations as 10, 20, 40 and 75 ppb. The stock solution is calibrated with 1000 ppm standard lead solution. The unknown concentrations of samples are calculated using the equation of the drawn calibration curve. The pH of the solutions after filtration and pH of DI water was measured by pH meter and found as 4.5 and 6.8, respectively. The measurements and their explanations are given in the following sections.

3.4.1. Pb^{+2} Adsorption on GO Depending on Time

The Pb^{+2} adsorption on GO was investigated depending on time to find the time where maximum adsorption is observed. GO was mixed with 50 ppm Pb^{+2} solution in mechanical stirrer and the samples were collected at 10 min, 20 min, 30 min, 50 min and 60 min. The collected samples were analyzed with ICP-MS to calculate the adsorbed Pb^{+2} concentration.

To measure the concentration of samples, first the calibration curve was drawn by using the standard solutions with concentrations 10 ppb, 20 ppb, 40 ppb and 75 ppb. The signals of standard solutions were measured with ICP-MS. The equation of the calibration curve was used for finding the concentration of the unknown samples. The data showing concentrations of standard samples and their corresponding cps are given in Table 3.5. For all measurements DI water was used as blank solution.

Table 3.6. Concentration of standard samples and their counts per second

Concentration (ppb)	cps	blank corrected cps
0	5,101	-
10	262,119	257,018
20	407,871	402,770
40	742,346	737,245
75	1,358,631	1,353,530

The calibration curve is drawn by using the known concentration of standards and their blank corrected cps data. The calibration graph is given in Figure 3.14. In the figure, x axis shows the concentration in ppb and the y axis shows the blank corrected cps data.

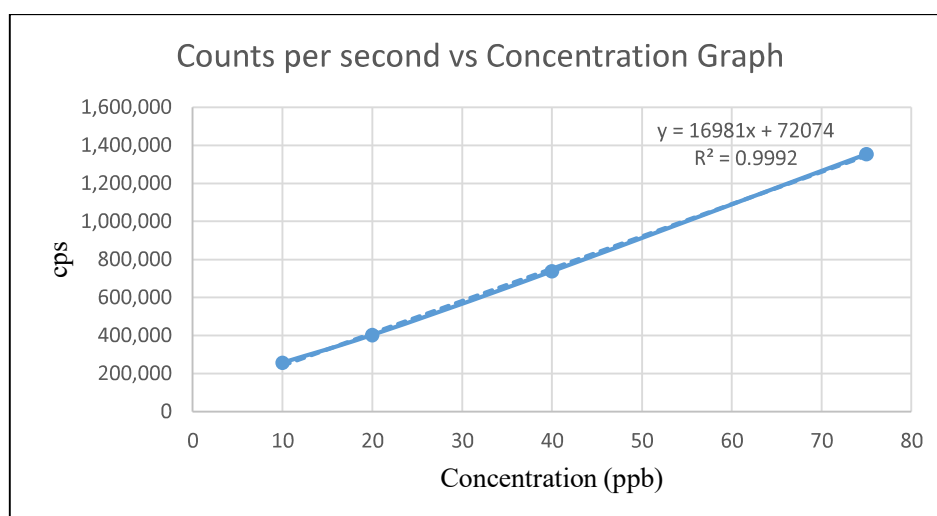


Figure 3.14. Graph of standard solutions cps vs concentration

To find the adsorbed Pb^{+2} amount on GO samples, the mass of Pb^{+2} put in the GO at the beginning was calculated. Total Pb^{+2} mass at the beginning in 50 ppm solution was;

$$\frac{50 \text{ mg}}{L} \times 0.025 \text{ L} = 1.25 \text{ mg } Pb^{+2}$$

The ICP-MS measurements give the non-adsorbed Pb^{+2} mass; therefore, this mass must be subtracted from the beginning Pb^{+2} mass. The table showing the initial, non-adsorbed and adsorbed Pb^{+2} concentrations is given in Table 3.7. The non-adsorbed mg of Pb^{+2} was calculated by substituting the cps data to the equation of the calibration graph. Then, these data were subtracted from the initial Pb^{+2} mass and the adsorbed Pb^{+2} mass was found.

Table 3.7. Adsorption of Pb^{+2} Samples on GO According to Time

Stirring Time with Pb^{+2} Solution (min)	Non-adsorbed Pb^{+2} (mg)	Adsorbed Pb^{+2} (mg)
10	0.99	0.26
20	0.59	0.66
30	0.21	1.03
50	0.54	0.71
60	0.19	1.06

The graph showing adsorption of Pb^{+2} on GO with respect to time is shown in Figure 3.15 and Table 3.7. From this graph, it is concluded that the adsorption of Pb^{+2} increases until 30 min and then decreases between 30 and 50 min and then increases again at 60 min. The difference for the 50 min data might be due to errors in experimental preparation or the inhomogeneous surface structure of GO. This shows that the maximum adsorption occurs between 30 and 60 min. Therefore, in the following experiments the GO and GO/TUT solutions were mixed for 60 min.

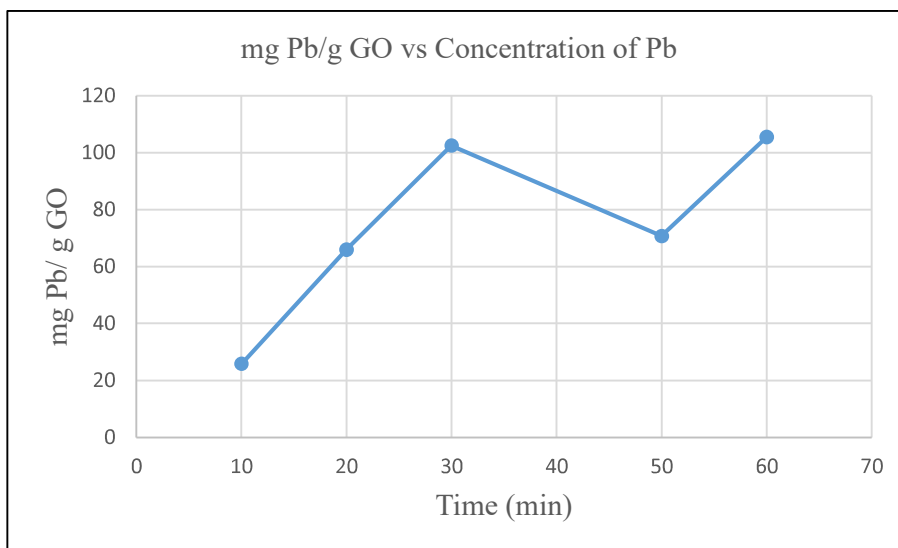


Figure 3.15. Graph showing adsorption of Pb^{+2} on GO depending on time

3.4.2. Pb^{+2} Adsorption Capacity of GO for Different Concentrations

Pb^{+2} adsorption on GO was studied at different concentrations of Pb^{+2} solutions as 25 ppm, 100 ppm, 250 ppm, 500 ppm, 750 ppm, 1000 ppm and 1500 ppm. Approximately 10 mg GO was put into these solutions. The exact weights of GO samples are given in Table 3.8. The solutions were stirred for 1 hour at room temperature and then the nonadsorbed lead concentration was measured with ICP-MS.

Table 3.8. Weight of GO Samples

Weight of GO (mg)	Concentration of Solution (ppm)
10.10	25
10.14	100
10.11	250
10.04	500
10.29	750
10.14	1000
10.33	1500

The non-adsorbed Pb^{+2} amount left in the solution was measured by ICP-MS by calculating the concentrations of samples using the cps data from the calibration curve. The adsorption capacity results for GO samples are given in Table 3.9. After calculating the non-adsorbed amount, it was subtracted from the initial mass and the adsorbed Pb^{+2} mass was found. Then this amount was divided to the gram of GO samples individually which were given in Table 3.8 to found $mg Pb^{+2}/g GO$.

Table 3.9. Adsorption capacity of GO with different concentrations of Pb^{+2}

Concentration (ppm)	Pb(mg) initial	Pb(mg) non-adsorbed	Pb(mg) adsorbed	mg Pb/g GO
25	0.625	0.03	0.59	58.5
100	2.50	1.39	1.11	109.1
250	6.25	2.68	3.57	352.8
500	12.5	4.94	7.56	752.6
750	18.75	9.25	9.50	923.3
1000	25.00	12.51	12.49	1231.9
1500	37.50	27.64	9.86	954.7

To find the maximum adsorption capacity of GO at different Pb^{+2} concentrations, a graph showing $mg Pb^{+2}$ adsorbed/ g GO vs concentration graph is drawn in Figure 3.16. From the graph, it is seen that the adsorption capacity of GO increases starting from 25 ppm to 1000 ppm. The maximum adsorption capacity per gram of GO is found at 1000 ppm. After this, the adsorption capacity decreases at 1500 ppm which shows that 1000 ppm solution which contains 25.0 mg Pb^{+2} has the highest adsorption amount for GO as approximately 1232 $mg Pb^{+2}/g GO$. The slight decrease at 1500 ppm might be due to the inhomogeneous structure of GO.

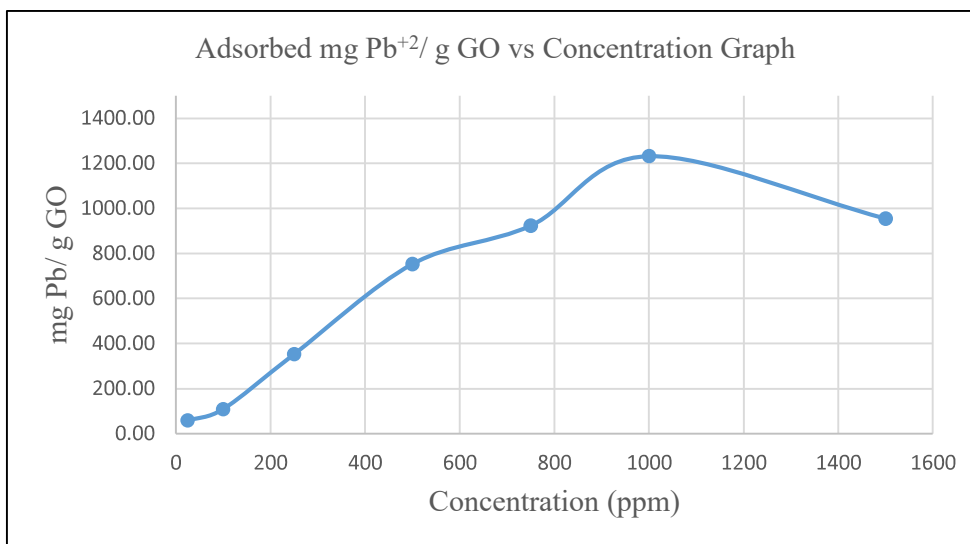


Figure 3.16. Adsorbed mg Pb²⁺/ g GO vs concentration graph

Since, the maximum adsorption capacity of GO is found at 1000 ppm concentration, the adsorption capacity of GO/TUT samples was studied at 1000 ppm Pb²⁺ concentration. The exact weights of GO/TUT samples are given in Table 3.10. The samples were mixed with 1000 ppm Pb²⁺ solution for 1 hour at room temperature and the non-adsorbed Pb²⁺ concentrations were measured by ICP-MS.

Table 3.10. Weight of GO/TUT samples

Sample Name	Weight (mg)
GO/TUT/5min	10.25
GO/TUT/40min	10.14
GO/TUT/50min	10.48
GO/TUT/60min	10.21
GO/TUT/3h	10.13
GO/TUT/24h	10.18
r-GO	10.29

Before calculating the data, a new calibration curve was drawn by the fresh prepared standard samples with concentrations 10 ppb, 20 ppb, 40 ppb and 75 ppb. The standard samples were prepared from the 10 000 ppm stock solution. First, 1000 ppm solution was prepared by taking 5.0 ml from 10 000 ppm stock solution and diluting with DI water to 50.0 ml. Then, 1.0 ppm solution was prepared by taking 50.0 μ l from 1000 ppm solution and diluting to 50.0 ml. The 1.0 ppm solution was used for preparing the standard solutions, 10 ppb, 20 ppb, 40 ppb and 75 ppb by taking respectively 500 μ l, 1.0. ml, 2.0 ml and 3.75 ml from 1 ppm Pb^{+2} solution and diluting to 50.0 ml. DI water was used as the blank solution. Standard solutions and their corresponding cps values are given in Table 3.11.

Table 3.11. *Standard samples and their cps data*

Concentration (ppb)	cps	blank corrected cps
0	1,597	-
10	190,013	188,416
20	318,133	316,536
40	587,416	585,819
75	1,065,241	1,063,644

The cps vs concentration graph is drawn in Figure 3.17. The slope was found as 13 498 and the intercept was found as 49 298. These data were used for finding the concentration of unknown samples. The cps data of the unknown sample is placed inside the equation as y value and the calculated x value gives the corresponding concentration of this solution. By this way, the non-adsorbed Pb^{+2} mass in the solutions were calculated.

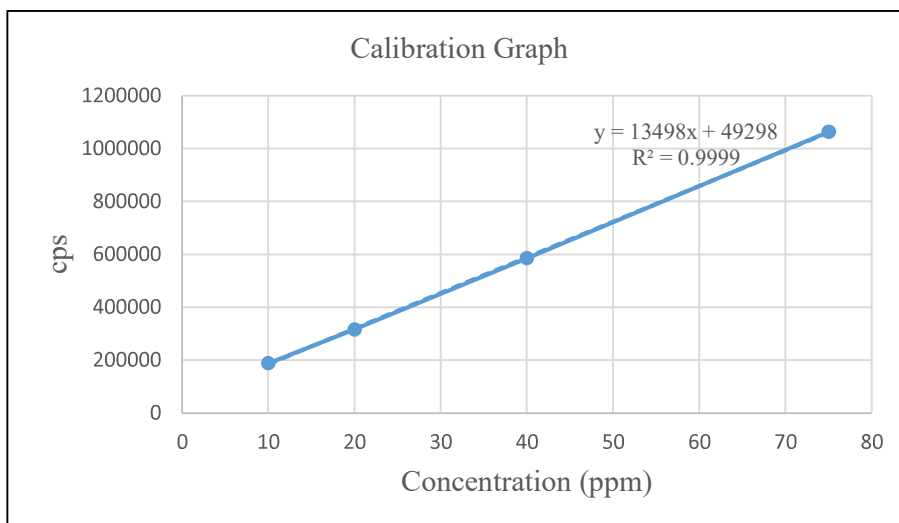


Figure 3.17. Standard samples cps vs concentration graph

As can be seen from Table 3.12, the highest Pb^{+2} adsorption capacity is obtained for GO/TUT/5min, which might be due to: a) existence of highest anchor points on the surface of sample and b) separation of stacks into individual layers. Therefore, GO/TUT/5min has the highest Pb^{+2} adsorption capacity. The smallest adsorption capacity was observed for GO/TUT/50min. It is believed that this is due to experimental difficulties, because it was not possible to obtain powder of GO/TUT/50min. The sample stucked together. Therefore, Pb^{+2} ion could not insert into the sample. The second smallest Pb^{+2} adsorption capacity is noted for r-GO, because of absence of attachment points on the surface of the sample, due to removal of functional groups from the sample.

Table 3.12. Adsorption Capacities of GO/TUT samples

	Pb(mg) initial	Pb(mg) non- adsorbed	Pb(mg) adsorbed	mg Pb/g GO	Adsorption Percentage (%)
GO	25	12.51	12.49	1232	50
GO/TUT/5min	25	4.1	20.9	2042	84
GO/TUT/40min	25	5.8	19.2	1891	77
GO/TUT/50min	25	17.1	7.9	752	32
GO/TUT/60min	25	7.5	17.5	1714	70
GO/TUT/3h	25	13	12	1188	48
GO/TUT/24h	25	6.8	18.2	1786	73
r-GO	25	17.1	7.9	763	31

The pH of the solutions measured after filtered with Chima Blue ribbon filter with pore size $\leq 2 \mu\text{m}$ and found as 4.5. The pH of the tap water was measured as 6.74. There are several studies that point out the effect of pH is important on adsorption capacity of GO. Sitko et al. reported that they found the highest adsorption capacity for GO at pH = 5 and the adsorption capacity increased between the pH= 3-5, remained approximately the same between pH = 5-8 [50]. Zhao et al. reported that the adsorption capacity increases up to pH=8 and then decreases [51]. Wang et al. reported the adsorption capacity for GO increases as the pH increased from 1 to 6, remains the same between pH 6-8 and decreases as pH becomes higher than 8 [88].

The pH effect on adsorption capacity is related with the form of Pb^{+2} at this pH. According to Sitko et al., the decrease of adsorption capacity at pH 6-8 is due to formation of PbOH^+ and $\text{Pb}(\text{OH})_2$ which have smaller positive charge making it hard for ion to adsorb on GO [50]. Wang et al. reported that at low pH values Pb^{+2} , after pH 5 PbOH^+ , after pH 7 $\text{Pb}(\text{OH})_2$ and at higher pH values $\text{Pb}(\text{OH})_3^-$ is found in the solution [88]. Therefore, at high pH positive charge on Pb^{+2} decreases and adsorption capacity decreases. All this information indicates that pH of the solution is important to define the Pb^{+2} ion adsorption capacity of the sample. Therefore, pH parameter should be investigated in the near future for these prepared samples.

In Table 3.13, GO prepared according to the Tour method showed a lower adsorption capacity than GO synthesized in this work. The FTIR spectrum is quite similar to the one in this study and the interlayer spacing was found as 8.26 Å [48]. They used maximum 60 ppm Pb⁺² solution which may be a low concentration to determine the adsorption capacity of GO. The difference of adsorption capacity might also occur due to some experimental differences during the reaction procedure. Raghubanshi et al. used 3.0 g graphite and 18 g of KMnO₄ and stirred for 18 hours [48]. In our study, we used 0.75 g graphite and 4.5 g KMnO₄ and stirred for 15 hours. Even the ratio of graphite to KMnO₄ is the same, the stirring time may not be enough for oxidizing all the graphite. Therefore, lower oxidation of layers may be a result of a lower adsorption capacity in their study. Also, Hummers method and Tour method gave different results in the literature. This might be due to NaNO₃ usage in Hummers method. If the GO solution is not washed and centrifuged enough, Na⁺ ions coming from NaNO₃ may settle between the layers and prevent Pb⁺² adsorption.

Table 3.13. Comparison of the results of this work with literature

Sample Name	Method or Chemical used	mg Pb ⁺² /g GO	Reference
GO	Tour	1232	Our results
GO/TUT/5min	Thiourea	2042	Our results
GO/TUT/40min	Thiourea	1891	Our results
GO/TUT/50min	Thiourea	752	Our results
GO/TUT/60min	Thiourea	1714	Our results
GO/TUT/3h	Thiourea	1188	Our results
GO/TUT/24h	Thiourea	1786	Our results
r-GO	Thiourea	763	Our results
GO	Hummers	30.13	[47]
GO	Tour	120	[48]
GO-AG	Hummers	789.9	[49]
GO	K ₂ Cr ₂ O ₇	1119	[50]
GO	Hummers	842	[51]

CHAPTER 4

CONCLUSION

In this thesis, GO, r-GO, GO/TUT/5min, GO/TUT/40min, GO/TUT/50min, GO/TUT/60min, GO/TUT/3h and GO/TUT/24h samples were synthesized, characterized with FTIR, XRD, TGA, UV-vis spectroscopy and SEM techniques and their Pb^{+2} adsorption capacities in aqueous solutions were measured with ICP-MS. GO/TUT/5min, GO/TUT/40min, GO/TUT/50min, GO/TUT/3h and GO/TUT/24h were prepared for the first time in this work.

The FTIR results indicated that thiourea might be attracted to the surface of GO through N and S atoms of thiourea.

The XRD pattern of GO demonstrated that it is composed of two planes; one is (100) plane ($2\theta=12.36^\circ$) with a large interlayer spacing (7.15 Å) due to insertion of oxygen containing functional groups between the layers and the other one is (002) plane of unoxidized graphene ($2\theta=23.54^\circ$) with a small interlayer distance (3.77 Å). The other prepared samples showed only one broad peak between 21° - 22° (2θ). The smallest interlayer space was observed for r-GO (3.87 Å) due to removal of functional groups from the surface of samples. The interlayer distance does not change much (~ 4.0 Å) for GO/TUT samples. The smallest number of layers (1.22) was obtained for GO/TUT/5min, indicating that it was almost completely exfoliated to the individual layers.

The TGA studies revealed that graphite itself is the most stable sample until 700°C . The r-GO showed good thermal stability compared to GO. GO indicated four weight losses according to a) adsorbed H_2O , b) labile oxygen containing functional groups, c and d) degradation of remaining functional groups. GO/TUT samples also showed

first weight loss for adsorbed water and then functional groups attached on the surface of samples.

In ICP-MS measurements indicated that GO/TUT/5min has the highest Pb^{+2} adsorption capacity (2042 mg Pb^{+2} /g GO/TUT/5min), which might be due to existence of highest anchor points on the surface of sample and separation of stacks (piles) into individual layers for GO/TUT/5min.

CHAPTER 5

FUTURE STUDIES

- a) Only one pH (4.5) solution medium has been studied for Pb^{+2} ion adsorption capacities of the prepared samples in this thesis. It is well known that the pH of the solution is quite effective for the Pb^{+2} adsorption capacities of the samples. Therefore, other pH mediums should be also investigated.

- b) BET and XPS measurements should be achieved to define the surface area of samples, oxidation states and environment of each atoms.

REFERENCES

- [1] A. M. Ghazi, J. R. Millette, *Environmental Forensics: Contaminant Specific Guide, Lead*, pp 55-79, 2007.
- [2] E. Wiberg, A. F. Holleman, N. Wieberg, *Inorganic Chemistry*, Academic Press, Chapter 5: Lead, pp 912-915, 2001.
- [3] Snow, B. D., & Project Muse, *Living with Lead: An Environmental History of Idaho's Coeur D'Alenes, 1885-2011, The Useful Metal, Brief History of Lead*, Pittsburgh, Pa: University of Pittsburgh Press, pp 37-46, 2017.
- [4] B. A. Fowler, Roles of lead binding proteins in mediating bioavailability, *Environmental Health Perspectives*, 106, 6, pp 1585-1587, 1998.
- [5] J. M. Ordemanna, R. N. Austin, *Lead neurotoxicity: exploring the potential impact of lead substitution in zinc-finger proteins on mental health*, *Metallomics*, 2016.
- [6] B. Quintanilla-Vega, D. R. Smitha, M. W. Kahng, J. M. Hernandez, A. Alboresc, B. A. Fowler, Lead-binding proteins in brain tissue of environmentally lead-exposed humans ³, *Chemico-Biological Interactions* 98 (1995) 193-209.
- [7] G. Richardt, G. Federolf, E. Habermann, Affinity of heavy metal ions to intracellular Ca⁺² binding proteins, *Biochemical Pharmacology*, 35, 8, 1331-1335, 1986.
- [8] J. P. Bressler, G. W. Goldstein, Mechanisms of lead neurotoxicity, *Biochemical Pharmacology*, 41, 4, 479-484, 1991.
- [9] M. Huang, D. Krepiy, W. Hu, D. H. Petering, Zn-, Cd-, and Pb-transcription factor IIIA: properties, DNA binding, and comparison with TFIIIA-finger 3 metal complexes, *Journal of Inorganic Biochemistry*, 2004, 98, 775-785.

[10] J. S. Magyar, O. T. Weng, C. M. Stern, D. F. Dye, B. W. Rous, J. C. Payne, B. M. Bridgewater, A. Mijovilovich, G. Parkin, J. M. Zaleski, J. E. Penner-Hahn, H. A. Godwin, Reexamination of Lead(II) Coordination Preferences in Sulfur-Rich Sites: Implications for a Critical Mechanism of Lead Poisoning, *Journal of American Chemical Society*, 2005, 127, 26, 9495-9505.

[11] ALAD gene aminolevulinatase dehydratase, 2019, March 19, Retrieved from <https://ghr.nlm.nih.gov/gene/ALAD>

[12] B. S. Gillis, Z. Arbieva, I. M. Gavin, Analysis of lead toxicity in human cells, *BioMed Central Genomics*, 2012, 13, 344, 1471-2164.

[13] I. D. de Souza, A. S. de Andradea, R. J. S. Dalmolin, Lead-interacting proteins and their implication in lead poisoning, *Critical Reviews in Toxicology*, 2018, 48, 5, 375–386.

[14] R. A. Goyer, Transplacental Transport of Lead, *Environmental Health Perspectives* 89, 101-105, 1990.

[15] A. Ghosh, S. Das, S. Kundu, P. K. Maiti, P. Sahoo, Rapid estimation of lead in lipsticks, *Sensors and Actuators B*, 2018, 266, 80-85.

[16] M. Vigeh, K. Yokoyama, Z. Seyedaghamiri, A. Shinohara, T. Matsukawa, M. Chiba, M. Yunesian, Blood lead at currently acceptable levels may cause preterm labour, *Occupational and Environmental Medicine*, 2011, 68, 231-234.

[17] Safe Drinking Water Committee, Commission on Life Sciences, Division on Earth and Life Studies, National Research Council, *Drinking Water and Health*, National Academies Press, 1977, 1.

[18] M. Tuzen, M. Soylak, K. Parlar, Cadmium and Lead Contamination in Tap Water Samples from Tokat, Turkey, *Bulletin of Environmental Contamination and Toxicology*, 2005, 75, 284-289.

- [19] M. Soylak, F. Armagan Aydin, S. Saracoglu, L. Elci, M. Dogan, Chemical Analysis of Drinking Water Samples from Yozgat, Turkey, *Polish Journal of Environmental Studies*, 2002, 11, 2, 151-156.
- [21] U. Çelik, J. Oehlenschlager, High contents of cadmium, lead, zinc and copper in popular fishery products sold in Turkish supermarkets, *Food Control*, 2007, 18, 258–261.
- [22] Y. Keskin, R. Baskaya, O. Özyaral, T. Yurdun, N. E. Lüleci, O. Hayran, Cadmium, Lead, Mercury and Copper in Fish from the Marmara Sea, Turkey, *Bulletin of Environmental Contamination and Toxicology*, 2007, 78, 258–261.
- [23] V. Morckel, Why the Flint, Michigan, USA water crisis is an urban planning failure, *Cities*, 2007, 62, 23–27.
- [24] B. Zietz, J. Dassel de Vergara, S. Kevekordes, H. Dunkelberg, Lead contamination in tap water of households with children in Lower Saxony, Germany, *The Science of the Total Environment*, 2001, 275, 19-26.
- [25] W. Peng, H. Li, Y. Liu, S. Song, A review on heavy metal ions adsorption from water by graphene oxide and its composites, *Journal of Molecular Liquids*, 2017, 230, 496-504.
- [26] F. Fu, Q. Wang, Removal of heavy metal ions from wastewaters: A review, *Journal of Environmental Management*, 2011, 92, 407-418.
- [27] M. A. Barakat, New trends in removing heavy metals from industrial wastewater, *Arabian Journal of Chemistry*, 2011, 4, 361–377.
- [28] L. Curkovic, S. Cerjan-Stefanovic, T. Filipan, Metal ion exchange by natural and modified zeolites, *Water Research*, 31, 6, pp 1379-1382, 1997.

- [29] J. Peric, M. Trgo, N. Vukojevic Medvidovic, Removal of zinc, copper and lead by natural zeolite-a comparison of adsorption isotherms, *Water Research*, 38, pp 1893-1899, 2004.
- [30] C. K. Brozek, L. Bellarosa, T. Soejima, T. V. Clark, N. Lopez, M. Dinca, Solvent dependent cation exchange in metal-organic frameworks, *Chemistry A European Journal Communication*, 20, pp 1-5, 2014.
- [31] M. Sabir, M. Zia-ur-Rehman, K. R. Hakeem, Saifullah, Phytoremediation of metal contaminated soils using organic amendments: Prospects and challenges, *Soil Remediation and Plants*, Chapter 17, pp 503-523, 2015.
- [32] Y. H. Li, S. Wang, J. Wei, X. Zhang, C. Xu, Z. Luan, D. Wu, B. Wei, Lead adsorption on carbon nanotubes, *Chemical Physics Letters*, 357, pp 263-266, 2002.
- [33] What is clinoptilolite? The industrialized one, Retrieved from <http://www.rotamining.com/clinoptilolite/> on 16th of May 2019.
- [34] N. L. Rosi, J. Eckert, M. Eddaoudi, D. T. Vodak, J. Kim, M. O'Keeffe, O. M. Yagh, Hydrogen storage in metal-organic frameworks, *Science*, 300, pp 1127-1130, 2003.
- [34] A. K. Geim, K. S. Novoselov, The rise of graphene, *Nature Materials*, 6, pp 183-191, 2007.
- [35] D. Bradley, A chemical history of graphene, *Carbon, Materials Today*, 2014.
- [36] B. C. Brodie, On the atomic weight of graphite, *Royal Society*, 149, pp 249-259, 1859.
- [37] R. A. Depine, *Graphene Optics: Electromagnetic Solution of Cononical Problems*, Chapter 5.11, Application Note-Graphene, pp 206-207, Morgan&Claypool, 2016.

[38] R. S. Edwards, K. S. Coleman, Graphene synthesis: relationship to applications, *Nanoscale*, 5, 38, pp 38-51, 2013.

[39] C. Lee, X. Wei, J. W. Kysar, J. Hone, Measurement of the elastic properties and intrinsic strength of monolayer graphene, *Science*, 321, pp 385-388, 2008.

[40] X. Huang, Z. Yin, S. Wu, X. Qi, Q. He, Q. Zhang, Q. Yan, F. Boey, H. Zhang, Graphene-based materials: synthesis, characterization, properties and applications, *Small*, 7, 34, pp 1876-1902, 2011.

[41] D.C. Markano, D. V. Kosynkin, J. M. Berlin, A. Sinitskii, Z. Sun, A. Slesarev, L. B. Alemany, W. Lu, J. M. Tour, Improved synthesis of graphene oxide, *ACS Nano*, 4, 8, pp 4806-4814, 2010.

[42] W. S. Hummers, R. E. Offeman, Preparation of Graphitic Oxide, *Journal of American Chemical Society*, 80, 6, pp 1339, 1958.

[43] C. K. Chua, M. Pumera, Monothiolation and reduction of graphene oxide via one-pot synthesis: hybrid catalyst for hydrogen reduction, *ACS Nano*, 9, 4, pp 4193-4199, 2015.

[44] X. Yang, Y. Wan, Y. Zheng, F. He, Z. Yu, J. Huang, H. Wang, Y. S. Ok, Y. Jiang, B. Gao, Surface functional groups of carbon-based adsorbents and their roles in the removal of heavy metals from aqueous solutions: A critical review, *Chemical Engineering Journal*, 366, pp 608-621, 2019.

[45] S. Wang, X. Li, Y. Liu, C. Zhang, X. Tan, G. Zeng, B. Song, L. Jiang, Nitrogen-containing amino compounds functionalized graphene oxide: Synthesis, characterization and application for the removal of pollutants from wastewater: A review, *Journal of Hazardous Materials*, 342, pp 177-191, 2018.

[46] D. Saha, S. Barakat, S. E. Van Bramer, K. A. Nelson, D. K. Hensley, J. Chen, Noncompetitive and Competitive Adsorption of Heavy Metals in Sulfur-

Functionalized Ordered Mesoporous Carbon, ACS Applied Materials and Interfaces, 8, pp 34132-34142, 2016.

[47] O. Olanipekun, A. Oyefusi, G. M. Neelgund, A. Oki, Adsorption of lead over graphite oxide, 118, pp 857-860, 2014.

[48] H. Raghubanshi, S. M. Ngobeni, A. O. Osikoya, N. D. Shooto, C. W. Dikio, E. B. Naidoo, E. D. Dikio, R. K. Pandley, R. Prakash, Synthesis of graphene oxide and its application for the adsorption of Pb^{+2} from aqueous solution, Journal of Industrial and Engineering Chemistry, 47, pp 169-178, 2017.

[49] W. Peng, H. Li, Y. Liu, S. Song Hu, Comparison of Pb(II) adsorption onto graphene oxide prepared from natural graphites: Diagramming the Pb(II) adsorption sites, Applied Surface Science, 364, pp 620-627, 2016.

[50] R. Sitko, E. Turek, B. Zawisza, E. Malicka, E. Talik, J. Heimann, A. Gagor, B. Feist, R. Wrzalik, Adsorption of divalent metal ions from aqueous solutions using graphene oxide, Dalton Transactions, 42, pp 5682-5689, 2013.

[51] G. Zhao, X. Ren, X. Gao, X. Tan, J. Li, C. Chen, Y. Huang, X. Wang, Removal of Pb(II) ions from aqueous solutions on few-layered graphene oxide nanosheets, Dalton Transactions, 40, pp 10945-10952, 2011.

[52] B. C. Smith, Fundamentals of Fourier Transform Infrared Spectroscopy, Second Edition, CRC Press, pp 1-53, 2011.

[53] D. A. Skoog, E. J. Holler, S. R. Crouch, Principles of Instrumental Analysis, Sixth Edition, International student edition.

[54] M. Eckert, Disputed discovery: the beginnings of X-ray diffraction in crystals in 1912 and its repercussion, Acta Crystallographica Section A, 68, pp 30-39, 2012.

[55] Choice of X-ray Target, Retrieved at 26.07.2019 from <http://pd.chem.ucl.ac.uk/pdnn/inst1/anode.htm>.

[56] A. A. Bunaciu, E. G. Udriștioiu, H. Y. Aboul-Enein, X-ray diffraction: instrumentation and applications, *Critical Reviews in Analytical Chemistry*, 45, 289-299, 2015.

[57] A. Monshi, M. R. Foroughi, M. R. Monshi, Modified scherrer's equation to estimate more accurately nano crystallite size using XRD, *World Journal of Nanoscience and Engineering*, 2, 154-160, 2012.

[58] A. Bogner, P. H. Jouneau, G. Thollet, D. Basset, C. Gauthier, A history of scanning electron microscopy developments: towards wet-STEM imaging, *Micron*, 38, pp 390-401, 2007.

[59] W. Zhaou, Z. L. Wang, Scanning microscopy for nanotechnology techniques and applications, chapter 1, Springer Verlag, first edition pp 1-40, 2007.

[60] M. Wagner, Thermal Analysis in Practice: Fundemantal Aspects, Carl Hanser Verlag GmbH & Co, Chapter 1, Introduction to Thermal Analysis, pp 10-15, 2017.

[61] P. S. Gill, S. E. Sauerbrunn, B. S. Crowe, High resolution thermogravimetry, *Journal of Thermal Analysis*, 38, pp 255-266, 1992.

[62] Thermogravimetric Analysis, Retrieved at 16.07.2019 from <https://pdfs.semanticscholar.org/5246/2cf71d854517dab1fdec4f52ab92bf6db26e.pdf>

[63] K. Mohomed, Thermogravimetric analysis (TGA) theory and applications, TA Instruments, Waters LLC.

[64] A. W. Coats, J. P. Redfern, Thermogravimetric analysis a review, *Analyst*, 88, pp 906-924, 1963.

[65] K. Satheesh, R. Jayavel, Synthesis and electrochemical properties of reduced grapheneoxide via chemical reduction using thiourea as a reducing agent, *Materials Letters*, 13, pp 5-8, 2013.

[66] B. Y. S. Chang, N. M. Huang, M. N. Anamt, A. R. Marlinda, Y. Norazriena, M. R. Muhamad, I. Harrison, H. N. Lim, C. H. Chia, Facile hydrothermal preparation of titanium dioxide decorated reduced graphene oxide nanocomposite, *Internal Journal of Nanomedicine*, 7, pp 3379-3387, 2012.

[67] T. Kuila, A. K. Mishra, P. Khanra, N. H. Kim, J. H. Lee, Recent advances in the efficient reduction of graphene oxide and its application as energy storage electrode materials, *Nanoscale*, 5, 52, 2013.

[68] M. Batsala, B. Chandu, B. Sakala, S. Nama, S. Domatoti, inductively coupled plasma mass spectrometry (ICP-MS), *International Journal of Research in Pharmacy and Chemistry*, 2, 3, pp 671-680, 2012.

[69] R. J. C. Brown, M. J. T. Milton, Analytical techniques for trace element analysis: an overview, *Trends in Analytical Chemistry*, 24, 3, pp 266-274, 2005.

[70] R. Thomas, A beginner's guide to ICP-MS, Part II sample introduction system, *Spectroscopy*, 16, 5, pp 56-60, 2001.

[71] W. Dunn, Mass spectrometry in systems biology: an introduction, *Methods in Enzymology*, Chapter two, 500, pp 15-35, 2011.

[72] P. Tan, J. Sun, Y. Hu, Z. Fang, Q. Bi, Y. Chen, J. Cheng, Adsorption of Cu^{+2} , Cd^{+2} and Ni^{+2} from aqueous single metal solutions on graphene oxide membranes, *Journal of Hazardous Materials*, 297, pp 251-260, 2015.

[73] Z. Ji, G. Zhu, X. Shen, H. Zhou, C. Wua, M. Wang, Reduced graphene oxide supported FePt alloy nanoparticles with high electrocatalytic performance for methanol oxidation, *New J. Chem.*, 36, pp 1774-1780, 2012.

[74] K. Satheesh, R. Jayavel, Synthesis and electrochemical properties of reduced graphene oxide via chemical reduction using thiourea as a reducing agent, *Materials Letters*, 113, pp 5-8, 2013.

[75] W. Chen, L. Yan, P. R. Ba, Chemical reduction of graphene oxide to graphene by sulfur-containing compounds, *J. Phys. Chem. C.*, 114, pp 19885–19890, 2010.

[76] Y. Wang, J. Liu, L. Liu, D. D. Sun, High-quality reduced graphene oxide nanocrystalline platinum hybrid materials prepared by simultaneous co-reduction of graphene oxide and chloroplatinic acid, *Nanoscale Research Letters*, 6, pp 241, 2011

[77] J. Porwal, N. Karanwal, S. Kaula, S. L. Jain, Carbocatalysis: N-doped reduced graphene oxide catalyzed esterification of fatty acids with long chain alcohols, *New J. Chem.*, 40, pp 1547-1553, 2016.

[78] J. Lu, Y. Li, S. Li, S. P. Jiang, Self-assembled platinum nanoparticles on sulfonic acidgrafted graphene as effective electrocatalysts for methanol oxidation in direct methanol fuel cells, *Scientific Reports*, 6, 21530, 2015.

[79] C. K. Chua, A. Ambrosi, M. Pumera, Graphene oxide reduction by standard industrial reducing agent: thiourea dioxide, *J. Mater. Chem.*, 22, 11054, 2012.

[80] Q. Lai, S. Zhu, X. Luo, M. Zou, S. Huang, Ultraviolet-visible spectroscopy of graphene oxides, *AIP Advances* 2, 032146, 2012.

[81] R. Su, S. F. Lin, D. Q. Chen, G. H. Chen, Study on the absorption coefficient of reduced graphene oxide dispersion, *The Journal of Physical Chemistry C*, 118, pp 12520 – 12525, 2014.

[82] Z. Tian, J. Li, G. Zhu, J. Lu, Y. Wang, Z. Shi, C. Xu, Facile synthesis of highly conductive sulfur-doped reduced graphene oxide sheets, *Phys. Chem. Chem. Phys.*, 18, pp 1125—1130, 2016.

[83] X. Wang, T. Liu, Fabrication and characterization of ultrathin graphene oxide/poly (vinyl alcohol) composite films via layer-by-layer assembly, *Journal of Macromolecular Science R, Part B: Physics*, 50, pp 1098–1107, 2011.

[84] L. Stobinska, B. Lesiaka, A. Malolepszy, M. Mazurkiewicz, B. Mierzwa, J. Zemek, P. Jiricek, I. Bieloshapka, Graphene oxide and reduced graphene oxide studied by the XRD, TEM and electron spectroscopy methods, *Journal of Electron Spectroscopy and Related Phenomena*, 195, pp 145–115, 2014.

[85] T. Alizadeh, F. Ahmadian, Thiourea-treated graphene aerogel as a highly selective gas sensor for sensing of trace level of ammonia, *Analytica Chimica Acta*, 897, pp 87-95, 2015.

[86] P. Bombicz, I. Mutikainen, M. Krunk, T. Leskela, J. Madarasz, Lauri Niinistö, Synthesis, vibrational spectra and X-ray structures of copper(I) thiourea complexes, *Inorganica Chimica Acta*, 357, pp 513–525, 2004.

[87] W. S. V. Lee, M. Leng, M. Li, X. L. Huang, J. M. Xuen, Sulphur-functionalized graphene towards high performance supercapacitor, *Nano Energy*, 12, pp 250–257, 2015.

[88] X. Wang, Z. Chen, S. Yung, Application of graphene oxides for the removal of Pb(II) ions from aqueous solutions: Experimental and DFT calculation, *Journal of Molecular Liquids*, 211, pp 957-964, 2015.